# 港湾技術研究所 報告

# 港湾技術研究所報告 (REPORT OF P. H. R. I.)

## 目　　次 (CONTENTS)

# 1. Mathematical Modeling of Mud Transport in Ports with a Multi-Layered Model —Application to Kumamoto Port—

Hiroichi TSURUYA*

Kazuo MURAKAMI**

Isao IRIE***

## Synopsis

A multi-layered model is developed for the prediction of mud transport in an estuary and ports. Extensive field measurements have been carried out in Kumamoto Port that is under construction to obtain detailed information on siltation mechanisms. A most remarkable result is the effect of a submerged dike on reducing the amount of deposition within the test trench.

A multi-layered model is adopted to take into account the effects of submerged dikes and to be able to reproduce the vertical distribution of suspended mud concentrations.

Numerical constants which govern mud transport, and the movement of mud layers by waves are estimated from the data obtained by the field observations and laboratory experiments. Finally, deposition rates in three trenches were used to calibrate the present model.

As the dimension of the trenches is 70×50m in area, the mesh size in and near them should be small, about 10m, but the area apart from these places doesn't need as fine a mesh. To satisfy such contradicting requirements, a nested grid model is adopted. The calculation is conducted with the supercomputer NEC SX-1E of the Port and Harbour Research Institute.

After the calibration of the deposition rates is completed, calculations for the future plans are carried out to estimate the amount of deposition for cases with and without submerged dikes.

It is predicted that submerged dikes 1m in height from the bottom will prevent siltation in the access channel and anchorages of Kumamoto Port by about 30% of the total deposition without submerged dikes

Key Words: Siltation, Kumamoto Port, Critical Shear Stress, Cohesive Sediment, Mud Transport.

* Chief of Hydrodynamics Laboratory, Marine Hydrodynamics Division
** Chief of Environmental Hydraulics Laboratory, Marine Hydrodynamics Division
*** Formerly, Director of Marine Hydrodynamics Division (Professor of Kyushu University)

# 1.　多層レベルモデルによる港湾埋没の
# 数値計算モデルの開発
### ——熊本港への適用例——

鶴谷広一\*・村上和男\*\*・入江　功\*\*\*

**要　　旨**

　シルテーションによる港湾や航路の埋没を予測するための数値計算プログラムを開発した。プログラムの主な特徴は，潜堤のような低い高さの構造物が海底に設置された場合を想定して，多層レベルモデルを採用したことである。このモデルによれば，現地と同様に底泥の濃度が鉛直に分布している状態も計算することができる。しかし，今回の計算のように7層という多層にすることによって，演算時間も飛躍的に大きくなるために，通常の計算機では実行不可能なため，港研で新しく導入したスーパーコンピュータ SX-1E を用いた。対象とした港は現在建設中の熊本港で，現地では埋没量観測用のトレンチが掘られ，同時に波，流れ，泥の濃度分布等が観測された。底泥の巻き上げや沈降にかかわる定数は，現地と実験室で得られたデータを用い，最終的にはトレンチで得られた埋没量に合うようにキャリブレーションを行った。このようにして，モデルの妥当性を確認した後，将来案に対する埋没量の予測と，潜堤を設置した場合の埋没量の軽減効果についての計算を行った。

　その結果，将来案1では，高さ1mの潜堤を建設することにより，埋没量が約30%減少し，将来案2では約23%埋没量が減少することがわかった。

**キーワード**：シルテーション，熊本港，限界せん断応力，粘着土，泥の移動

---

　　\* 海洋水理部水理研究室長
　\*\* 海洋水理部海域環境研究室長
\*\*\* 前海洋水理部長（現九州大学工学部）

# CONTENTS

# 1. Introduction

Mud processes in an estuary are comprised of many factors such as flocculation, deposition, consolidation, and erosion. In estimating the amount of mud deposition in harbours and access channels, numerical simulations are a useful method. Although mud processes are termed as 'siltation', physical processes included in the siltation vary considerably from place to place. Consequently, we must be aware of the natural conditions in the field where we are concerned; e. g. bed materials, waves, currents, salinity, etc.

Extensive field measurements have been carried out in Kumamoto Port which is under construction to obtain detailed information on siltation mechanisms. A most remarkable result is the effect of a submerged dike on reducing the amount of deposition within the test trench.

A multi-layered model is adopted to take into account the effects of submerged dikes and to be able to reproduce the vertical distribution of suspended mud particles.

Numerical constants which govern mud transport process are estimated from the data obtained by the field observations and laboratory experiments. Finally, deposition rates within three trenches were used to calibrate the present model.

As the dimension of the trenches is 70m×50m in area, the mesh size around them should be small, about 10m, but the area apart from these places doesn't need as fine a mesh. To satisfy such contradicting requirements, a nested grid model is adopted. The calculation is conducted with the supercomputer NEC SX-1E of the Port and Harbour Research Institute.

After the calibration of the deposition rates is completed, calculations for the future plans are carried out to estimate the amount of deposition for cases with and without submerged dikes.

It is predicted that submerged dikes 1 m in height from the bottom will prevent siltation in the access channel and anchorages of Kumamoto Port by about 30% of the total deposition without submerged dikes.

# 2. Mathematical Modeling of Mud Transport

## 2.1 General Outline of the Model

External forces governing mainly the mud movement and transport in an estuary are tidal currents, wave-induced currents, and waves. As the coastal area around Kumamoto Port consists of a wide shoal of soft mud, the range of the shoreline movement is about 2km or more. The model must be able to take this movement into account. Moreover, it is expected that the model can treat the detailed configuration of the bed and construction such as submerged dikes. Consequently, we adopted the multi-layered model with nested grid for the calculation of tidal currents and diffusion of bed materials including erosion and deposition.

The present model consists of several horizontal layers as shown in Fig. 1. The effect of the structure on the siltation, (e. g. submerged dikes) can be reasonably evaluated by the present model. The submerged dikes are to be constructed at 4 m to 7 m below the MWL. By taking this into consideration, the water depth is vertically divided into seven layers as shown in Fig. 2. The nested grid model can treat the composite arrangement of rough and fine meshes.
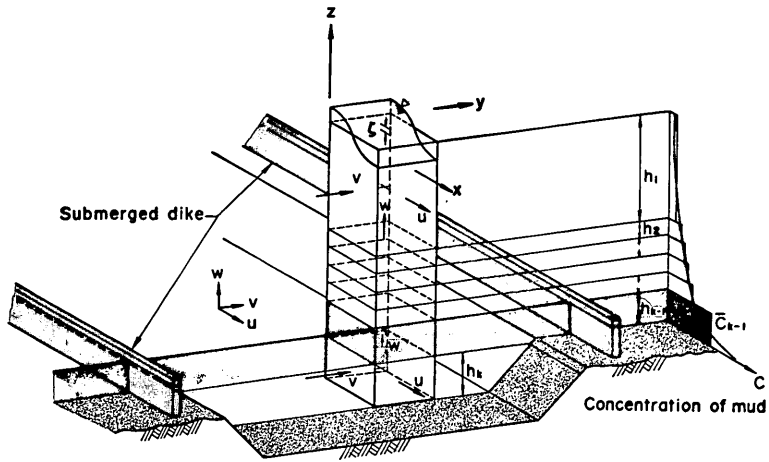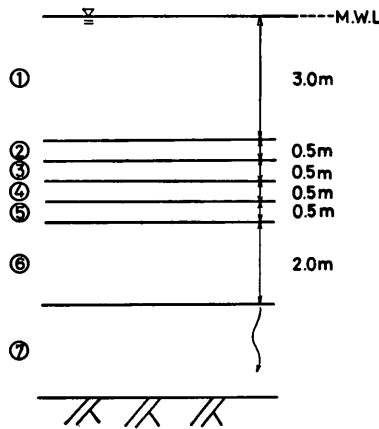
**Fig. 1** Multi-Layered Level model



**Fig. 2** Division of Water Depth into
Seven Layers

The supercomputer NEC SX-1E is used for the calculation. It takes, however, four hours to calculate 24 hours of tidal currents in the field.

**2. 2 Basic Equations**

Tidal currents on a shoal are calculated by a set of known equations: (1) continuity equations, and (2) equations of motion. Mud is transported in suspension and this process can be represented by diffusion equations.

**( 1 ) Continuity equations**

The continuity equation for the total layer is expressed as

$$\frac{\partial \zeta}{\partial t}+\frac{\partial}{\partial x}(\sum_{k=1}^{Kmax} M_k)+\frac{\partial}{\partial y}(\sum_{k=1}^{Kmax} N_k)=0, \quad\quad\quad (1)$$

where, $\zeta$ is the water surface elevation, $M_k$ and $N_k$ ($=uh_k$, $vh_k$) are the horizontal fluxes in the $x$ and $y$ directions, respectively, $u$ and $v$ are the horizontal mean velocities

in the $x$ and $y$ directions, respectively, $h_k$ the thickness of layers, $K_{max}$ the number of layers, and subscript $k$ denotes the $k$-th layer. For each layer, the condition of continuity must be also satisfied and the equation can be written as

$$w_{k-1/2} + \frac{\partial}{\partial x} M_k + \frac{\partial}{\partial y} N_k = w_{k+1/2}, \qquad \cdots\cdots\cdots\cdots\cdots\cdots (2)$$

where, $w$ is the vertical velocity. Variables in the equations are illustrated in Fig. 1.

(2) Equations of Motion

Equations of motion for each layer in the $x$ and $y$ directions are expressed as

$$\frac{\partial M_k}{\partial t} + \frac{\partial (Mu)_k}{\partial x} + \frac{\partial (Mv)_k}{\partial y} + (wM|_{k-1/2} - wM|_{k+1/2})/h_k$$

$$= fN_k - \frac{h_k}{\rho_k} \frac{\partial p_k}{\partial x} + A_x \frac{\partial^2 M_k}{\partial x^2} + A_y \frac{\partial^2 M_k}{\partial y^2} \qquad \cdots\cdots\cdots (3)$$

$$+ h_k \left[ \frac{\gamma^2 (u_{k-1}-u_k) \Delta U_{k-1/2}}{h_{k-1/2}} - \frac{\gamma^2 (u_k-u_{k+1}) \Delta U_{k+1/2}}{h_{k+1/2}} \right],$$

and

$$\frac{\partial N_k}{\partial t} + \frac{\partial (Nu)_k}{\partial x} + \frac{\partial (Nv)_k}{\partial y} + (wN|_{k-1/2} - wN|_{k+1/2})/h_k$$

$$= -fM_k - \frac{h_k}{\rho_k} \frac{\partial p_k}{\partial y} + A_x \frac{\partial^2 N_k}{\partial x^2} + A_y \frac{\partial^2 N_k}{\partial y^2} \qquad \cdots\cdots\cdots (4)$$

$$+ h_k \left[ \frac{\gamma^2 (v_{k-1}-v_k) \Delta U_{k-1/2}}{h_{k-1/2}} - \frac{\gamma^2 (v_k-v_{k+1}) \Delta U_{k+1/2}}{h_{k+1/2}} \right],$$

where $\rho$ is the density which is the function of salinity ($s$) and suspended solids ($SS$), $f$ the *Corioli's* parameter, $p$ the pressure, $A_x$ and $A_y$ are the horizontal eddy viscosities in the $x$ and $y$ directions, respectively, $g$ the acceleration of gravity, $\gamma^2$ the friction coefficient ($\gamma_b^2 = gn^2/h^{1/6}$ for the bottom layer), $n$ the *Manning's* roughness coefficient, and

$$\Delta U_{k-1/2} = \sqrt{(u_{k-1}-u_k)^2 + (v_{k-1}-v_k)^2}.$$

*Irie and Kuriyama* (1988) have demonstrated the importance of vertical distribution of the currents in mathematical modeling of the morphological changes in harbours.

(3) Mass Conservation Equations (for salinity and $SS$)

Conservation of mass stands for both salinity ($s$) and suspended solids ($SS$). Mass conservation equations are expressed as

$$\frac{\partial (C_k h_k)}{\partial t} = -\frac{\partial}{\partial x} (M_k C_k) - \frac{\partial}{\partial y} (N_k C_k) - (w+w_s)C|_{k-1/2} + (w+w_s)C|_{k+1/2}$$

$$+ \frac{\partial}{\partial x} \left(K_x h_k \frac{\partial C_k}{\partial x}\right) + \frac{\partial}{\partial y} \left(K_y h_k \frac{\partial C_k}{\partial y}\right) + \left(K_z \frac{\partial C}{\partial z}\right)_{k-1/2} - \left(K_z \frac{\partial C}{\partial z}\right)_{k+1/2}, \qquad \cdots (5)$$

where, $C$ is the mean concentration, $K_x$, $K_y$, and $K_z$ are horizontal in the $x$ and $y$ directions and vertical diffusion coefficients, respectively, and $w_s$ the settling velocity of mud particles. The vertical arrangement of variables for the multi-layered level model is shown in Fig. 3.
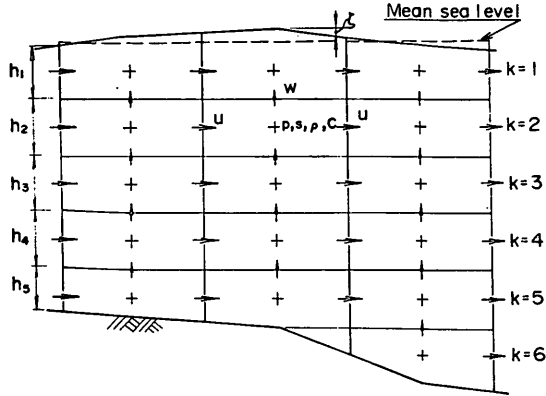
Fig. 3   Vertical Arrangement of Variables

( 4 )   Nearshore Currents

Nearshore currents induced by waves are calculated by using the continuity equation (1) and the equations of motion in which the radiation stress terms $M_x$ and $M_y$, as well as the bottom friction terms $F_x$ and $F_y$ are included.

The radiation stress terms $(M_x, M_y)$ are given by the following equations as

$$M_x = -\frac{1}{\rho}\left(\frac{\partial S_{xx}}{\partial x} + \frac{\partial S_{xy}}{\partial y}\right),$$

$$M_y = -\frac{1}{\rho}\left(\frac{\partial S_{xy}}{\partial x} + \frac{\partial S_{yy}}{\partial y}\right),$$

$$\cdots\cdots\cdots\cdots\cdots\cdots\cdots\cdots\cdots\cdots\cdots\cdots\cdots\cdots\cdots (6)$$

where $\rho$ is the density of water, $S_{xx}$, $S_{xy}$, $S_{yy}$ are the radiation stress components and the expressions for which are

$$S_{xx} = E n_w \left\{ (1+\cos^2\theta) - \frac{1}{2}\right\},$$

$$S_{xy} = E\frac{n_w}{2}\sin 2\theta,$$

$$S_{yy} = E n_w \left\{ (1+\sin^2\theta) - \frac{1}{2}\right\},$$

$$\cdots\cdots\cdots\cdots\cdots\cdots\cdots\cdots\cdots\cdots\cdots (7)$$

where $\theta$ is the direction of wave propagation, $n_w = C_g/C_w$, $C_k$ the group velocity, $C_w$ the wave celerity, $E = \rho g H^2/8$, and $H$ is the wave height.

The bottom friction terms $(F_x, F_y)$ owing to waves and currents are estimated by the following equations as

$$F_x = F \left\{M (1+\cos^2\theta) + \frac{N}{2}\sin 2\theta\right\},$$

$$F_y = F \left\{M (1+\sin^2\theta) + \frac{N}{2}\sin 2\theta\right\},$$

$$\cdots\cdots\cdots\cdots\cdots\cdots\cdots\cdots\cdots\cdots (8)$$

where $F = f_w H/\{T\sinh (k_w h)\}$, $f_w$ the Jonsson's friction coefficient (Jonsson, 1966), $T$ the wave period, $k_w$ the wave number, $h$ the water depth, and $M$ and $N$ are discharge components in the $x$ and $y$ directions, respectively.

**(5) Deformation of Waves**

Random sea wave refraction is calculated by solving the energy flux equation which contains wave damping owing to interaction between surface waves and mud beds. The fundamental equation takes the form

$$\frac{\partial}{\partial x}(Sv_x) + \frac{\partial}{\partial y}(Sv_y) + \frac{\partial}{\partial \theta}(Sv_\theta) + 2k_iC_gS = 0, \quad \cdots\cdots\cdots\cdots\cdots\cdots (9)$$

where $S$ denotes the directional wave spectral density, $k_i$ the damping coefficient owing to interaction (*Tsuruya et al.*, 1987), and $v_x$, $v_y$, and $v_\theta$ which are given by

$$
\begin{aligned}
v_x &= C_g\cos\theta, \\
v_y &= C_g\sin\theta, \\
v_\theta &= \frac{C_g}{C}\left(\frac{\partial C}{\partial x}\sin\theta - \frac{\partial C}{\partial y}\cos\theta\right),
\end{aligned}
\quad \cdots\cdots\cdots\cdots\cdots\cdots (10)
$$

where $C$ and $C_g$ denote phase and group velocities, respectively.

Wave damping by random wave breaking is given by *Goda* (1985). Diffraction and reflection of random waves are calculated by *Takayama's* method (1981).

**2.3 Mud Transport Model**

Physical processes governing the transport of cohesive sediment in estuaries are settlement, deposition, erosion, convection, diffusion, and consolidation.

In Kumamoto Port, abrupt deposition occurrs during stormy weather. This type of deposition is expected to be reproduced in the calculation. Consolidation process, therefore, is not considered in the present model because the time scale of the consolidation is much larger than that of the abrupt deposition.

**(1) Erosion**

In the model, bottom materials are separately treated as mud and sand. The rate of erosion from the bed ($E$) is given as a boundary condition of the mass conservation equations (5). The rate of erosion of mud has been formulated by *Partheniades* (1965) as

$$E = M\left(\frac{\tau_b}{\tau_e} - 1\right), \quad \cdots\cdots\cdots\cdots\cdots\cdots\cdots\cdots\cdots\cdots\cdots\cdots (11)$$

where $\tau_b$ (Pa) is the shear stress at the bottom by the combined action of waves and currents, $\tau_e$ (Pa) the critical shear stress for erosion, and $M$ (kg/m$^2$/min) is the constant. The bottom shear stress $\tau_b$ is given by *Tanaka and Shuto* (1981).

The rate of erosion of sand can be expressed by *Bijker's* formula (1980, 1982) as

$$E_s = K_z\left(\frac{C_{KMAX} - C_B'}{\frac{h_{KMAX}}{2}}\right), \quad \cdots\cdots\cdots\cdots\cdots\cdots\cdots\cdots\cdots (12)$$

where $C_{KMAX}$ is the concentration of sand at the bottom layer, $C_B'$ is the concentration of sand at the bed given by $C_B$ (*Bijker*, 1980, 1982) and the weight proportion (Eq.17), $h_{KMAX}$ the thickness of the bottom layer, $K_z$ ($=0.16V_{*cw}h/100$) the vertical diffusion coefficient, $V_{*cw}$ the bed shear velocity owing to waves and currents, $h$ the water depth, and $C_B$ which is expressed as

$$C_B = \frac{S_bC_h}{6.34\ Vr\sqrt{g}}, \quad \cdots\cdots\cdots\cdots\cdots\cdots\cdots\cdots\cdots\cdots\cdots\cdots (13)$$

where $S_b$ is the bead load and is given by the following relation as

$$S_b = \frac{Bd_{50}V\sqrt{g}}{C_h} \exp\left[\frac{-0.27 \Delta d_{50}C_h^2}{\mu V^2 \{1 + \frac{1}{2}(\frac{\xi u_w}{V})^2\}}\right], \qquad \cdots\cdots\cdots\cdots\cdots\cdots (14)$$

where $C_h$ is the resistance coefficient after *Chezy* and equal to $18\log(12h/r)$ with $r$ as the apparent bed roughness, $V$ the mean velocity, $B (\fallingdotseq 5)$ the coefficient, $d_{50}$ the grain size of the bed material, $\Delta$ the relative density of the bed material, $\mu$ the ripple coefficient, $n$ the *Manning's* roughness coefficient, $u_w$ the amplitude of the horizontal orbital velocity at the bed, and $\xi$ which is expressed as

$$\xi = C_h\sqrt{\frac{f_w}{2g}}, \qquad \cdots\cdots\cdots\cdots\cdots\cdots\cdots\cdots\cdots\cdots\cdots\cdots\cdots\cdots (15)$$

where $f_w$ is the friction coefficient as derived by *Jonsson* (1966).

Contributions of the weight proportion from mud and sand can be estimated by

$$E_m = P_m E, \qquad \cdots\cdots\cdots\cdots\cdots\cdots\cdots\cdots\cdots\cdots\cdots\cdots\cdots\cdots (16)$$

$$C_B' = P_s C_B, \qquad \cdots\cdots\cdots\cdots\cdots\cdots\cdots\cdots\cdots\cdots\cdots\cdots\cdots (17)$$

where $P_m$ and $P_s$ are the weight proportions of mud and sand in the bed, respectively, and $E_m$ and $E_s$ in Eq. (12) are erosion rates of mud and sand taking the weight proportion into account.

( 2 ) Deposition

Deposition rate $D$ is estimated by a similar consideration by *Sheng and Lick* (1979) as

$$\begin{aligned}D &= w_s C_{bed} \\ &= \beta w_s C_{KMAX}, \end{aligned} \qquad \cdots\cdots\cdots\cdots\cdots\cdots\cdots\cdots\cdots\cdots\cdots\cdots (18)$$

where $w_s$ is the settling velocity, $C_{bed}$ the concentration of mud at the bed, and $\beta$ is the correction factor to estimate $C_{bed}$ from the mean concentration of the bottom layer ($C_{KMAX}$).

From the calculation, we can obtain the mean concentration $C_{KMAX}$ at the bottom layer, but we want to know the concentration near the bed. The correction factor $\beta$ is introduced to estimate the concentration near the bottom from the calculated mean concentration $C_{KMAX}$. The factor $\beta$ may depend on the wave conditions, turbulence, the type of bed materials, and the thickness of the bottom layer. It is, therefore, extremely difficult to get an universal expression for $\beta$. We now estimate the value of $\beta$ from the field observation data. Figure 4 shows the typical distribution of SS observed at the observation tower and the pipe pile on August 31st, 1987. Plotted data are the average values of SS measured by water samplers. Detailed description will be given on 3.4 (4). Fitted curves are exponential functions and the concentraion at the bed is assumed to be the average value from the bed to the height of 5 cm. Estimated value of $\beta$ for each observation station are also shown in the figure as a function of the thickness of the bottom layer. Because of the exponential distribution, the value of $\beta$ decreases as the thickness of the bottom layer increases. Moreover, it is suspected from the measured data at two stations that the value of $\beta$ varies from place to place. In the calculation, however, it is unrealistic to give different values of $\beta$. Here we assume that the value of $\beta$ is given by the average value obtained at the observation station and the pipe pile, and $\beta$ is constant if the thickness of the bottom
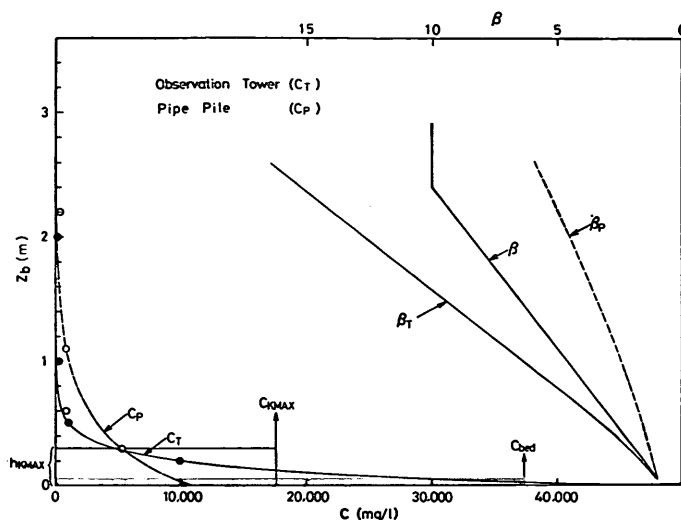
Fig. 4  Vertical Distributions of SS and $\beta$

layer is larger than 2.36 m.    The thick solid line in Fig. 4 shows the functional relationship between the thickness of the bottom layer and $\beta$, given by the following expression as

$$\beta = \begin{cases} 1.0, & (z_b \leq 0.05\text{m}) \\ 3.9z_b + 0.805, & (0.05 < z_b \leq 2.36\text{m}) \\ 10.0, & (z_b > 2.36\text{m}) \end{cases} \quad \cdots\cdots\cdots\cdots\cdots\cdots\cdots\cdots\cdots \quad (19)$$

where $z_b$ is the height from the bed and equal to the thickness of the bottom layer $h_{KMAX}$.

( 3 )  Settling Velocity

The settling velocity $w_s$ for sand in the *Bijker's* model is given by *Rubey's* formula (1933) as a function of the grain size.    For mud, on the other hand, $w_s$ depends on the concentration of mud.    As the concentration increases, a probability of collision between mud particles increases and the settling velocity increases.    Above some specific concentration, the settling velocity begins to decrease because of the hindered settling (*Dyer*, 1986).

The relationship stated above is schematically shown in Fig. 5.    The relationship between the settling velocity and the concentration of mud is expressed as

$$\begin{aligned} w_s &= A_1 C^{B_1}, (C < C_H) \\ &= A_1 C_H{}^{B_1} [1 - A_2 (C - C_H)]^{B_2}, (C \geq C_H) \end{aligned} \quad \cdots\cdots\cdots\cdots\cdots\cdots\cdots\cdots \quad (20)$$

where $A_1$, $A_2$, $B_1$, $B_2$, and $C_H$ are empirical constants.    *Mehta* (1986) has given the values of these constants for the field data in Severn Estuary (*Thorn*, 1981).    The broken line in Fig. 5 is given by *Mehta*.

In the present model, hindered settling is not effectively applied because details of the process are not yet known.    Here we assumed that the settling velocity is constant for the concentration greater than the critical value $C_H$.    Two asterisks in the figure are obtained by solving the diffusion equation in which the convection and diffusion terms are neglected.    The measured time variation of vertical distribution of turbidity
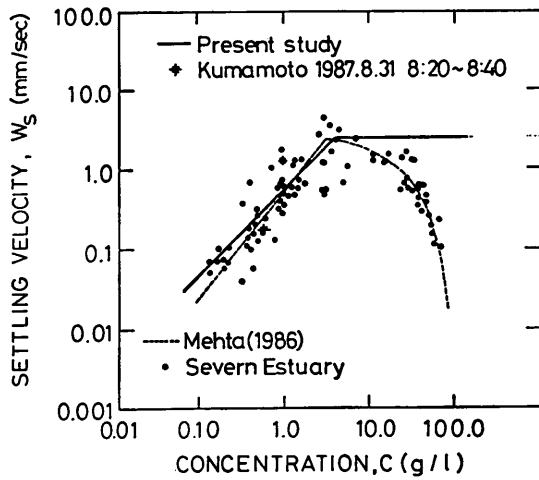
**Fig. 5** Relation between Settling Velocity
and Concentration of Mud

in the field will be discussed later.

( 4 ) Diffusion Coefficients behind Submerged Dikes

Turbulence intensity in the region behind a submerged dike increases considerably. Vertical and horizontal diffusion coefficients also increase when compared with cases without submerged dikes (*Tsuruya et al.*, 1987). The rate of increase in the diffusion coefficients with and without submerged dikes is given by

$$\frac{K_H}{K_{H0}} = [\frac{U_m}{U_{ref}} (K_H' - 1.0) + 1.0], \qquad \cdots\cdots\cdots\cdots\cdots\cdots\cdots\cdots\cdots\cdots\cdots\cdots \quad (21)$$

where $K_H$ is the diffusion coefficient behind a submerged dike, $K_{H0}$ the diffusion coefficient without a submerged dike, $U_m$ the mean velocity in the second layer, $U_{ref}$ the velocity at the reference point, and $K_H'$ is the rate of increase in the diffusion coefficient which is given by the experiment (Fig. 6).
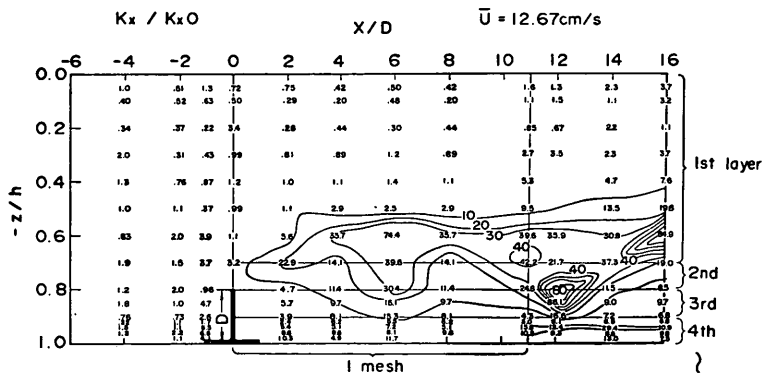


**Fig. 6** Rate of Increase in Horizontal Diffusion Coefficient

## 3. Natural Conditions on the Eastern Side of Ariake Bay and Field Observations at Kumamoto Port

For the simulation of mud transport, it is necessary to obtain data on the natural conditions by field observations. These are tides, tidal currents, winds, waves, and bed material properties such as particle size distributions, water contents, critical shear strength, and other characteristics which are related to mud transport. In this chapter, natural conditions, bed material properties, and results of the field observations during stormy weather are described. All these field observations are conducted by the Fourth District Port Construction Bureau, Ministry of Transport (*Yatsushiro Port Construction Office*, 1988).

### 3.1 Natural Conditions on the Eastern Side of Ariake Bay

Kumamoto Port is under construction as a new commercial port at a site off-Kumamoto City in Ariake Bay as shown in Fig. 7. Ariake Bay is surrounded by
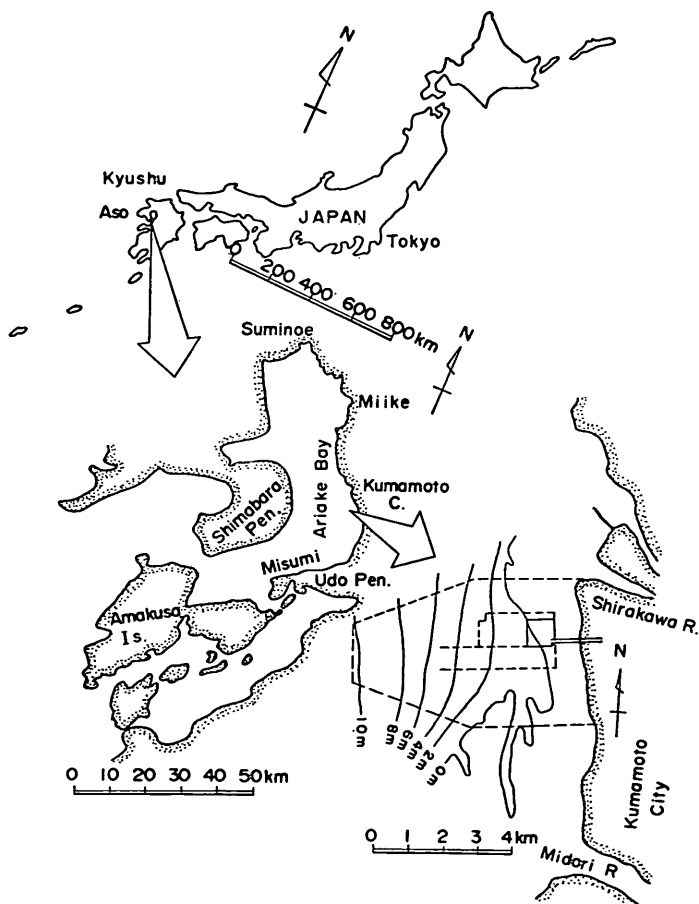


Fig. 7 Construction Site of Kumamoto Port
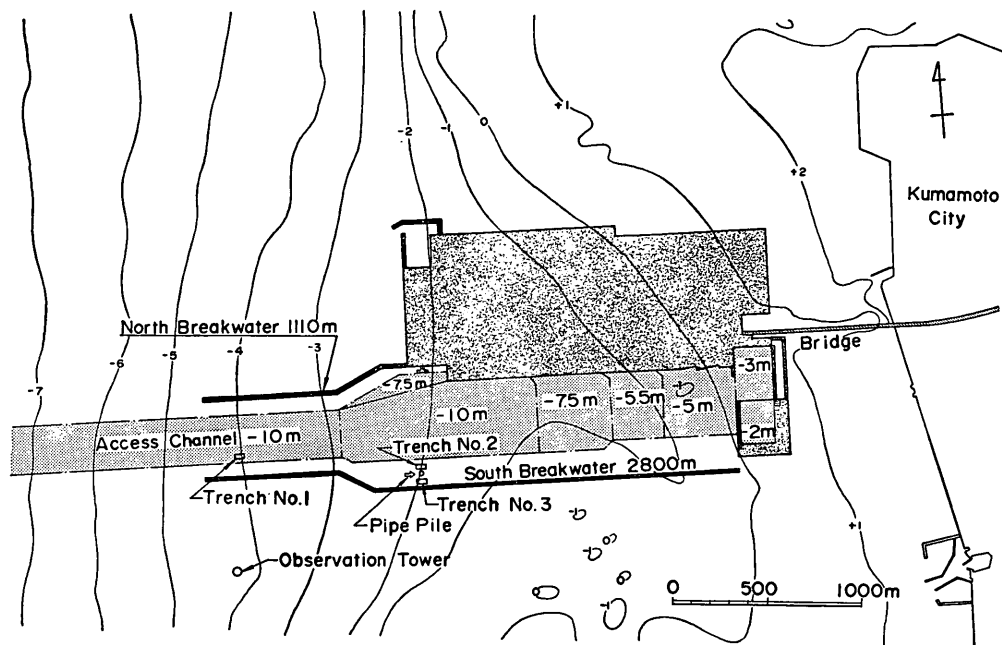
Fig. 8   Plan of Kumamoto Port and Field Observation Site

Shimabara Peninsula, Udo Peninsula, Amakusa Islands, and the Kumamoto Coast.   The tidal range here is highest of all the Japanese coast.   Owing to the geographical conditions, tidal currents are strong and wave heights are small compared with other Japanese coasts.

There are two main rivers flowing into the Kumamoto Port area.   These rivers originate in the Aso Mountains, which is a famous active volcano.   A great amount of fine sediment is transported from the mountain area to Ariake Bay.   As a result of the fine sediment discharge, a wide tidal flat has been formed in front of Kumamoto City. Therefore, it is thought that the area is not suitable for the construction of a port because of siltation problems.   However, a new port which is accessible from Kumamoto City has been projected, because the city has become a center of trade and industry of the Central Kyushu District.

The Fourth District Port Construction Bureau has carried out many kinds of field observations about siltation around the construction site to establish sufficient counter-measures against siltation.

Figure 8 shows the final plan of Kumamoto Port.   The observation tower and the pipe pile which are shown by open circles were built at 4 m and 2 m depths, respectively, below the LWL to measure tides, waves, winds, and turbidity of sea water.
(1)   Tides

Tides are a fundamental factor to determine the natural conditions such as water surface elevation, tidal currents, etc. in an enclosed inner bay.   Ariake Bay is famous for the highest tidal range in the Japanese coast.   Harmonic constants in several ports within Ariake Bay are shown in Table 1.   Wave induced water particle velocity at the bottom is a function of the water depth, as is the breaking wave height.   Therefore,

**Table 1**  Harmonic Constants of Ports in Ariake Bay

| Station | Kumamoto | | Mi-ike | | Suminoe | | Misumi | |
|---|---|---|---|---|---|---|---|---|
| Tidal Component | Amp. (H) | Phase ($\kappa$) | Amp. (H) | Phase ($\kappa$) | Amp. (H) | Phase ($\kappa$) | Amp. (H) | Phase ($\kappa$) |
| Sa | 17.64 | 140.64 | 20.73 | 139.19 | 19.0 | 148.0 | 19.35 | 144.71 |
| Ssa | 4.47 | 20.70 | 4.02 | 352.68 | — | — | 1.92 | 328.45 |
| $O_1$ | 21.17 | 197.30 | 21.96 | 199.24 | 21.6 | 205.0 | 20.92 | 198.22 |
| $K_1$ | 28.06 | 217.48 | 28.96 | 218.66 | 26.7 | 221.1 | 27.27 | 218.22 |
| $M_2$ | 134.68 | 255.08 | 155.38 | 259.28 | 172.1 | 267.1 | 121.19 | 253.35 |
| $S_2$ | 57.90 | 290.68 | 68.09 | 294.96 | 74.8 | 305.9 | 52.03 | 288.15 |

the wave-induced shear stress acting on the bed is considerably influenced by the water surface level.

A tide gauge has been installed on the tower at a depth of 4 m since 1975. The harmonic constants at the site of the tower are shown in Table 1. Figure 9 shows the several kinds of tidal levels at Kumamoto Port based on the harmonic constants data collected from December, 1975 to January, 1977.
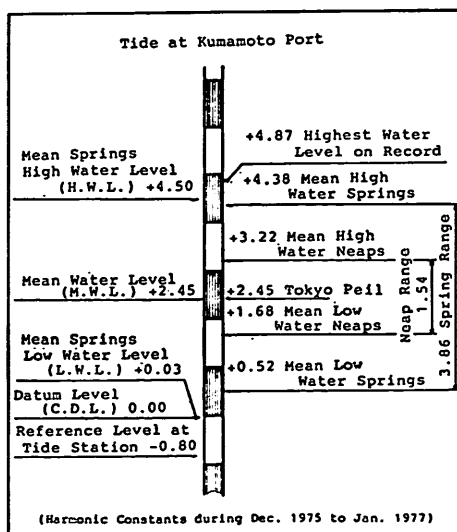


Fig. 9  Tidal Properties Diagram at Kumamoto Port

（2） Tidal Currents

Tidal currents were observed by three Anderra-type current meters and three Ono-type current meters.   Sea bottom sediments are eroded by the shear stress caused by tidal currents and wave action.   The suspended materials are then transported by tidal currents.   Tidal currents, therefore, play an important role in transporting bed materials. Field measurements of tidal currents were carried out at the six observation stations as shown by the triangeles in Fig.10. Continuous measurements for 15 days were carried out at three stations (solid triangles) in Fig. 10.   At the open triangles in the same figure, observations for 1 day were carried out.   Observed tidal current pattern in the spring tide are shown in Figs. 11 (a) to 11 (l).   Generally speaking, the south-west direction current is predominant at edd tide and the north-east direction current is predominant at flood tide.   The maximum velocity is in the range from 30 to 50 cm/s.
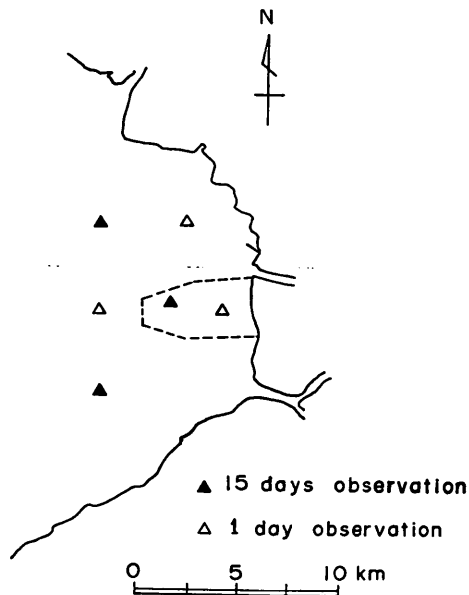


**Fig. 10** Observation Stations of Tidal Currents
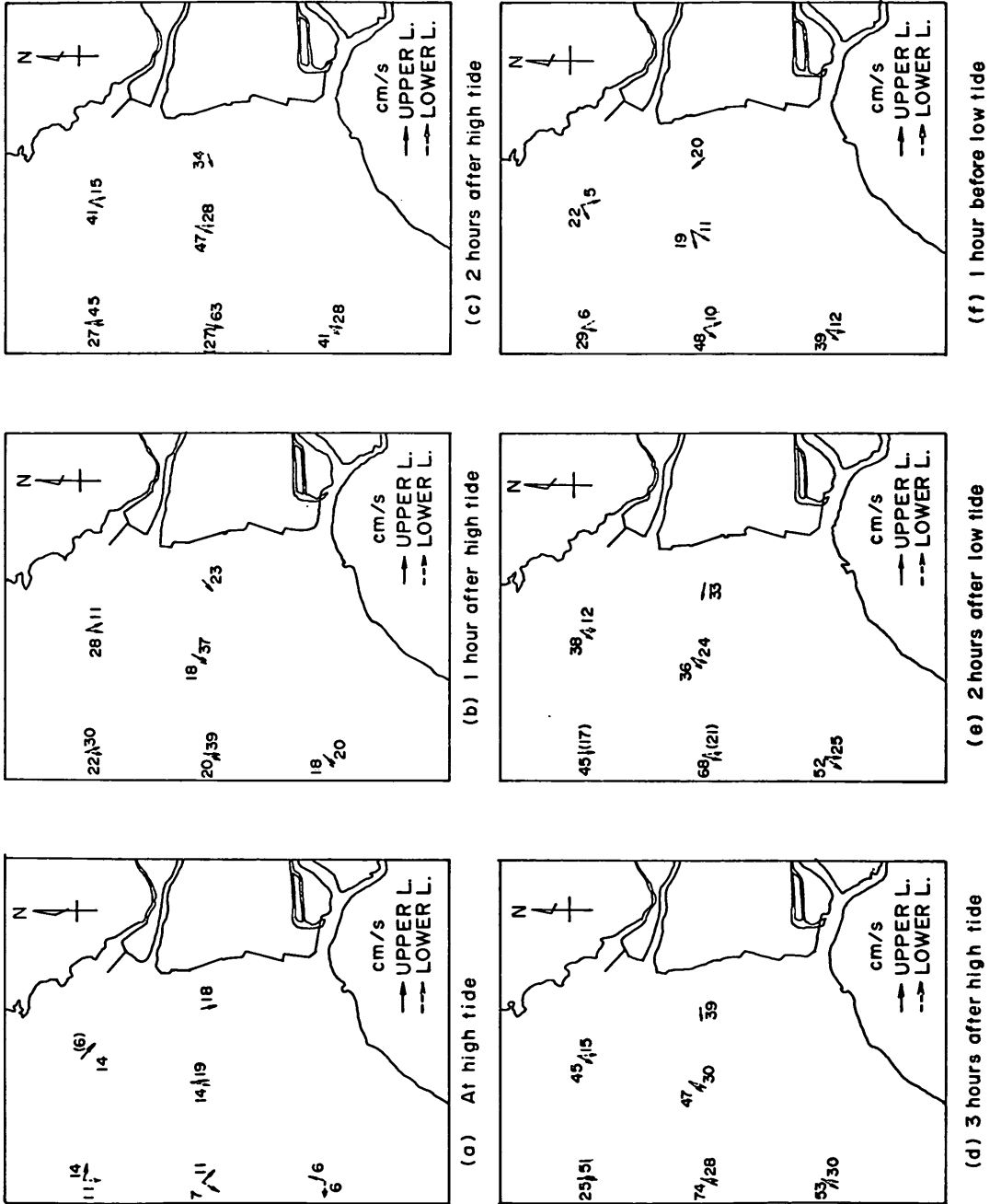
Fig. 11 ( a )   Tidal Current Pattern
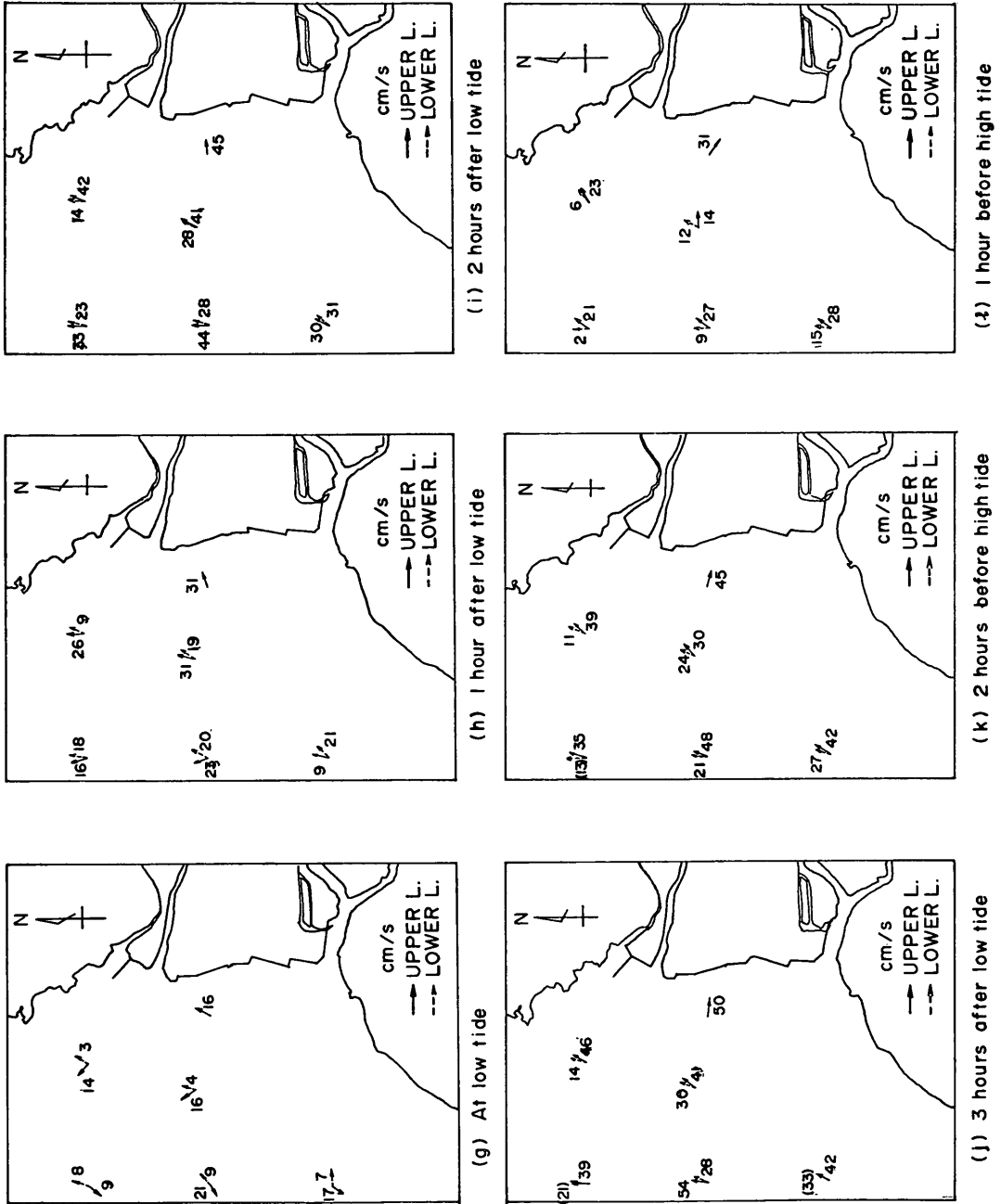
Fig. 11 (b)  Tidal Current Pattern

(3)　Winds

An anemometer is fixed on the observation tower.　Figure 12 shows the diagrams of frequency distributions of wind direction (wind rose) in a whole year, in winter season, and in summer season.　In winter season, the direction of the predominant winds stronger than 10m/s, caused by monsoons, is from North to North-North-West. In summer season, the main cause of strong winds are typhoons, so the predominant wind direction is not determined.　The fetch length is an important factor for the generation of wind waves.　Figure 13 shows the fetch lengths from the opposite side coast of Kumamoto Port, in which fetch lengths from North-West and South-West are longest.　In Kumamoto Port, therefore, wind directions from North-West and South-West are important.

(1)　Four seasons　　　　　(2)　Winter seasons　　　　　(3)　Summer seasons



Legend
☐ 0.3~4.9 m/sec
▨ 5.0~9.9　〃
▧ 10.0~14.9　〃
■ 15.0~19.9　〃
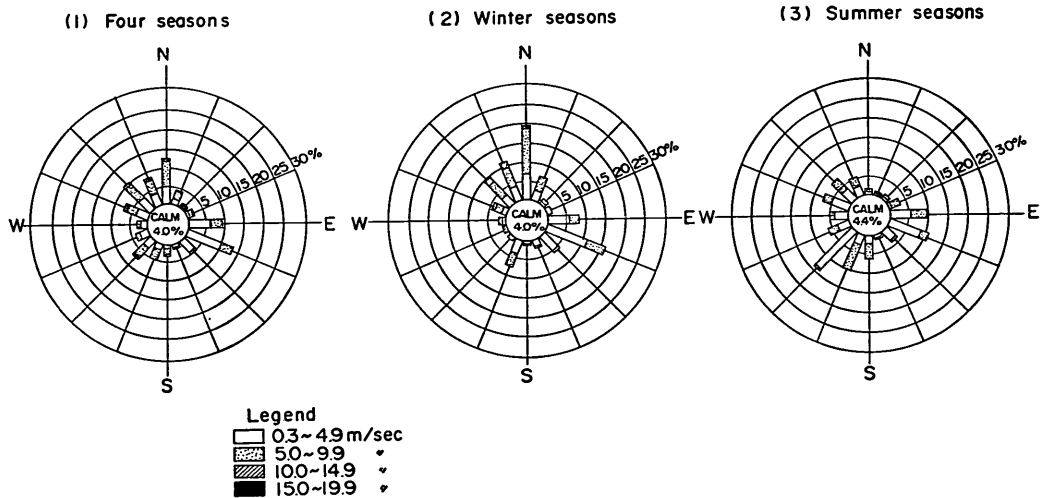
Fig. 12　Wind Roses
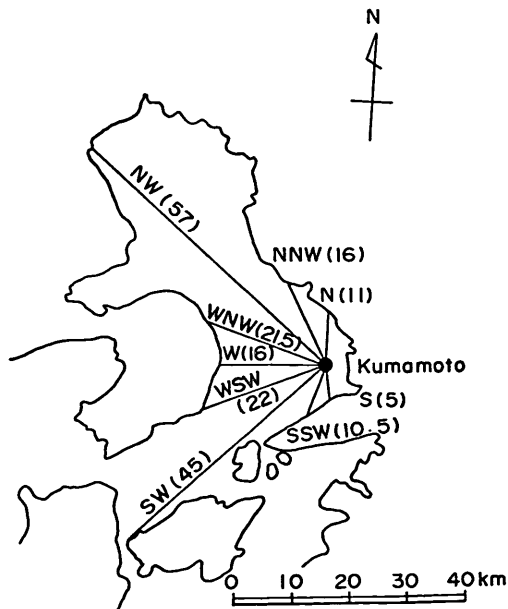


Fig. 13　Fetch Lengths of Kumamoto Port
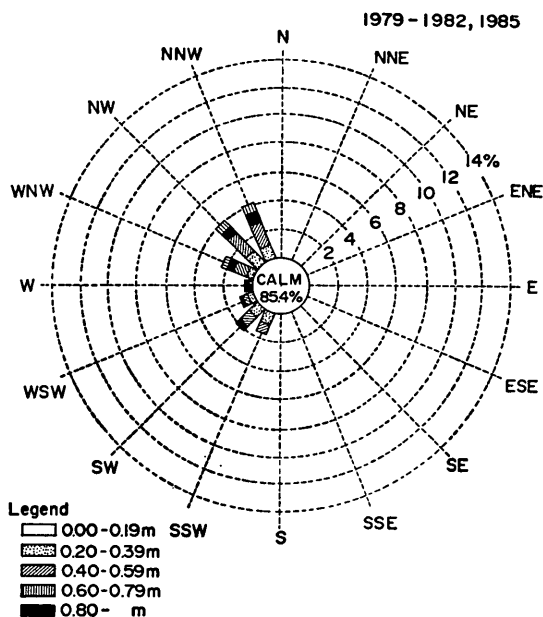
Fig. 14 Frequency Distributions of Wave Heights
in Each Direction

(4) Waves

Waves are significant external forces for the erosion of bottom sediments in Kumamoto Port.  As the swells from the ocean cannot enter Ariake Bay because of the enclosed configuration, almost all waves that attack Kumamoto Port are wind generated within Ariake Bay.

Figure 14 shows the frequency distributions of wave height in each wave direction for a whole year.  According to Fig. 14, wave directions of large waves are North-West to North-North-West.  This is because of the monsoons in winter.

3. 2  **Properties of Bed Materials in Kumamoto Port**

In considering siltation, properties of bed materials are important factors as well as natural conditions.  In order to graps the characteristics of bottom materials, bottom samplings are carried out in the observational area.  Figures 15(a) and 15(b) show the horizontal distributions of the main constitution of soil materials and its water content. Bottom sediments in the offshore area have high water content and small particle size. Therefore, the bed materials in the offshore side consist of fine clay and silt.  On the other hand, bottom sediments in the onshore side have low water content and large particle size.  The bed materials in the onshore side consist of fine sand and silt.  The lead penetration records at each location correspond to the water content and other properties of the bottom materials.
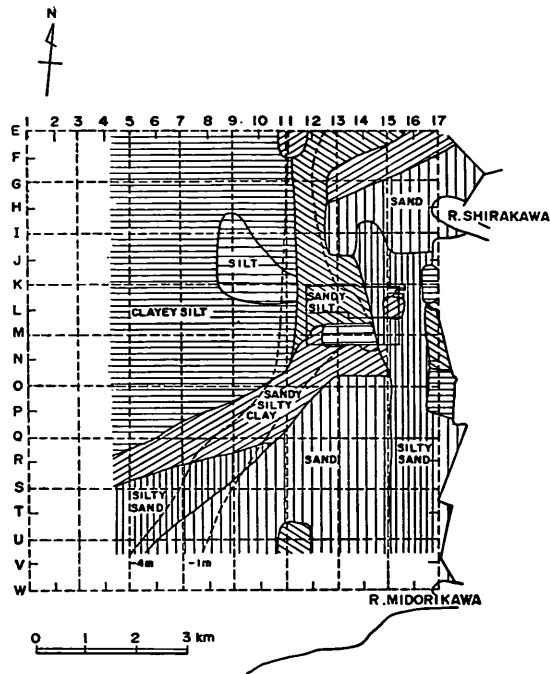
Fig. 15 (a)　Horizontal Distribution of Main
　　　　　　　Constitution of Soil Materials
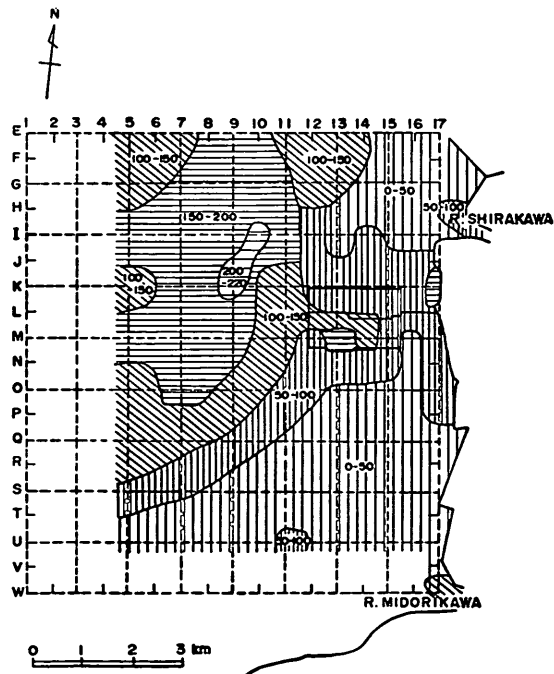


Fig. 15 (b)　Horizontal Distribution of Water
　　　　　　　Content of Soil Materials (%)

## 3.3 Field Observation Site and Measurement Equipment

In the previous sections, general characteristics of natural conditions and bottom sediment properties are described. However, there still remains the relationship between external forces and the sediment movement. In Kumamoto Port, the bottom sediment erosion is mainly caused by stormy waves. Synthetic field observations are, therefore, carried out during stormy weather.

Three trenches are constructed to investigate the relationship between the amount of sediment deposition and external forces such as waves and currents. The effect of a submerged dike to reduce the amount of deposition is also tested. Three trenches are shown in Fig. 8. Trench No. 1 is located at 4 m depth below LWL, and trenches No. 2 and 3 are located at 2 m depth below LWL. Trench No. 3 is surrounded by a submerged dike of 1 m in height. On the other hand, No. 2 trench is surrounded by no facility. Trenches No. 2 and 3 are located 100 m apart from each other. The scale of these trenches is 70 m in length and 50 m in width with a rectangular shape. The depth of the trenches is 2 m from the bed level and the side slope is 20%. Figure 16 shows the side and plane views of these trenches with and without the submerged dike.

Various field measurements are performed around the trenchec as shown in Table 2. The pipe pile for the tentative observation is constructed between trenches No. 2 and No. 3. At a depth of 4 m, there is an observation tower for long period observation. Figure 17 shows the observation tower and the measuring instrument fixed on a pile. Similar measuring instrument is equipped on the pipe pile. Other measurement equipment is set in the trenches as shown in Fig. 18.

Since it is considered that the deposition would be predominant during stormy
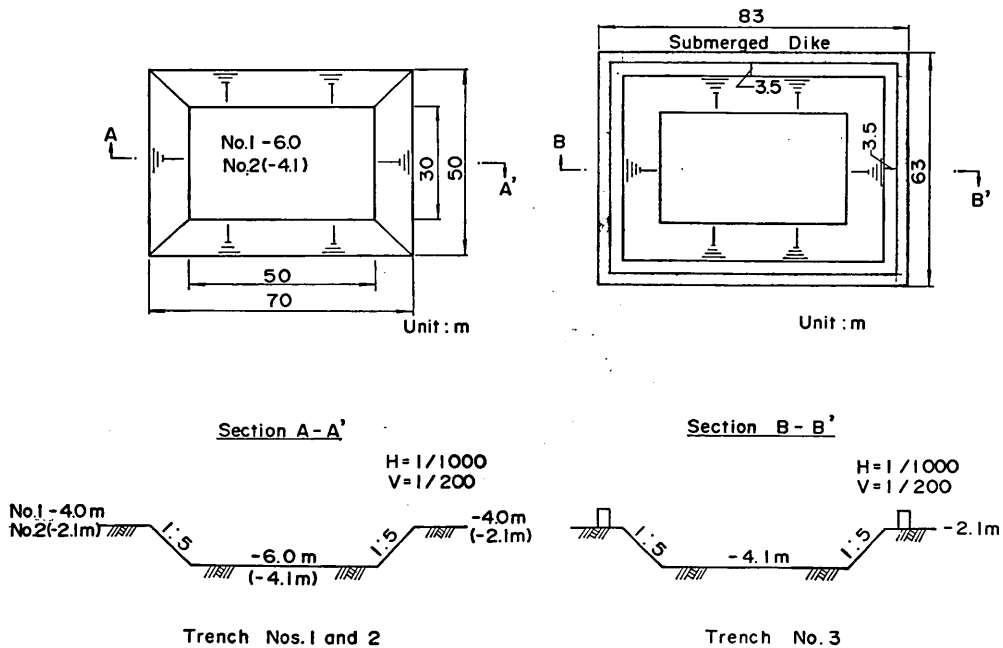


Fig. 16 Side and Plane Views of Trenches

Mathematical Modeling of Mud Transport in Ports with a Multi-Layered Model

Table 2  Field Survey Items

| Items | Equipment | Location |
|---|---|---|
| Siltation volume | Echo sounding<br>Measuring pole | 3 trenches |
| Currents | Electro-magnetic current<br>meter | 2 trenches and tower and<br>pipe pile |
| Suspended Solids | Water sampler | Tower and pipe pile |
| Turbidity | Turbidity meter (optic) | Tower and pipe pile |
| Waves | Ultra-sonic wave gauge | Tower |
| Bottom surface | Sand level meter | 2 trenches |
| Tide | Tide gauge | Tower |
| Sediment properties | Sediment sampler | 3 trenches |
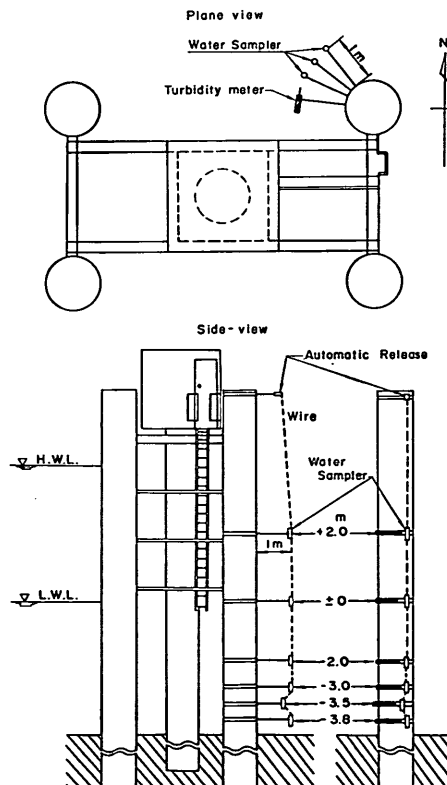


Fig. 17  Observation Tower and Measuring Equipment
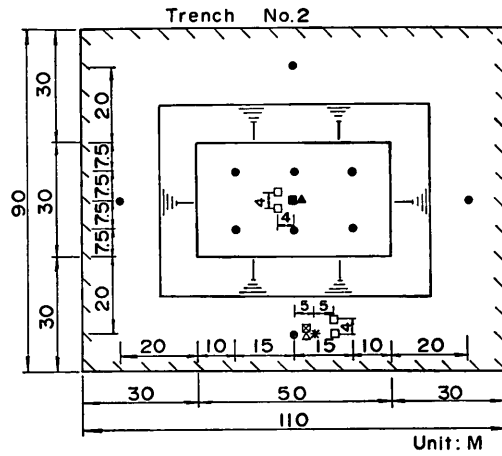
Fig. 18  Measuring Equipment in Trenches

weather, water sampling and turbidity measurement were carried out at the observation tower and the observation pile automatically during the onset of typhoon and large wave conditions.  Water samplers and turbidity meters are equipped with the observation tower and the pipe pile as shown in Fig. 17.

### 3.4  Results of Field Measurement

(1)  Weather conditions during observation period

During the observation period from December 1986 to March 1988, there were only several occasions when significant wave height $H_{1/3}$ exceeded 1.0 m.  Table 3 shows

Table 3  Typical High Wave Records during Rough Weather

| Date | Time | Significant wave height | wave period | Duration exceeds 0.7m |
|---|---|---|---|---|
| 1987. 2.  3 | 16 | 1.14 m | 4.4 s | |
| | 18 | 1.25 m | 4.9 s | 30 hours |
| | 20 | 1.03 m | 4.2 s | |
| 1987. 8. 31 | 0 | 1.14 m | 3.4 s | |
| | 2 | 1.33 m | 4.2 s | |
| | 4 | 1.69 m | 5.3 s | 14 hours |
| | 6 | 1.25 m | 4.9 s | |

the observed large waves during this period. In winter monsoon season, large significant wave heights from 1.03 to 1.25 m were observed. The corresponding significant wave period was about 4.5 second. The dominant wave direction was North-West. The time during which the significant wave heights exceeded 0.7 m lasted about 30 hours.

In the summer season, typhoon No. 8712 set upon the area. Large significant wave heights greater than 1.6 m were observed. However, the time during which the significant wave height exceeded 0.7 m was shorter than the monsoon season.

( 2 ) Siltation Volume in Trenches

Inside the three trenches, ten poles were set to measure the increase of bottom levels owing to the deposition of bed materials. Figure 19 shows the time variation of
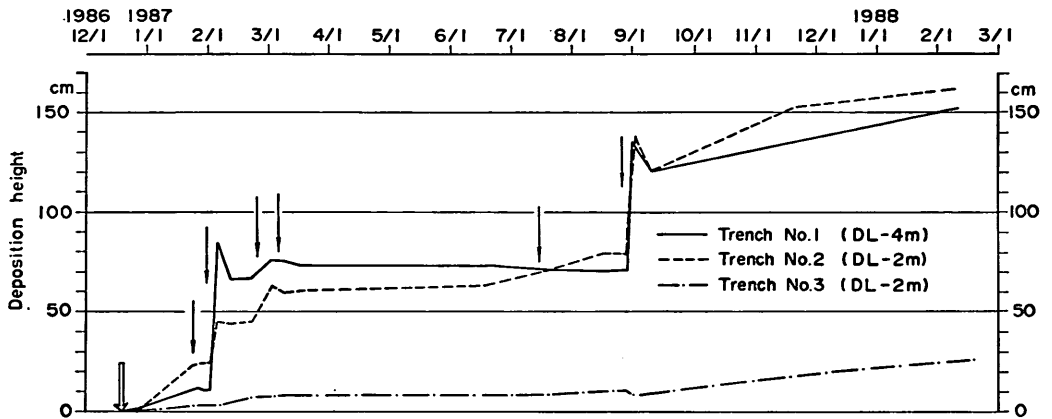


Fig. 19 Time Variation of Deposition Heights at the Center of Three Trenches
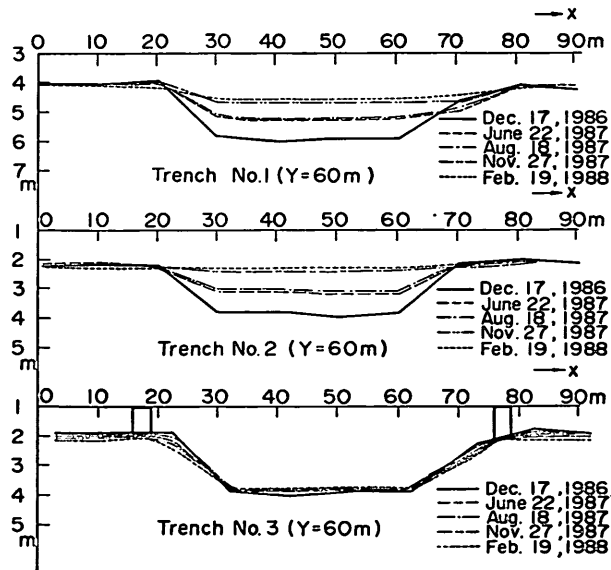


Fig. 20 Time Variation of Bottom Profiles within each Trench

deposition heights at the center of each trench. In the figure, six arrows show the onest of large waves. The leftmost arrow shows the start of the observation. It is found from the figure that the severe and sudden deposition occurred at trenches No. 1 and No. 2 during rough seas on February 3rd, 1987 and on August 31st, 1987, On the other hand, the deposition at trench No.3 was small. It is considered that the submerged dike has a considerable effect on reducing the deposition of mud. During gentle and calm seas, a small amount of deposition occurred in three trenches. This fact means that the tidal current has little effect on the deposition.

Figure 20 shows the time variations of bottom profiles within each trench from

From Aug 30 to Sep 3, 1987
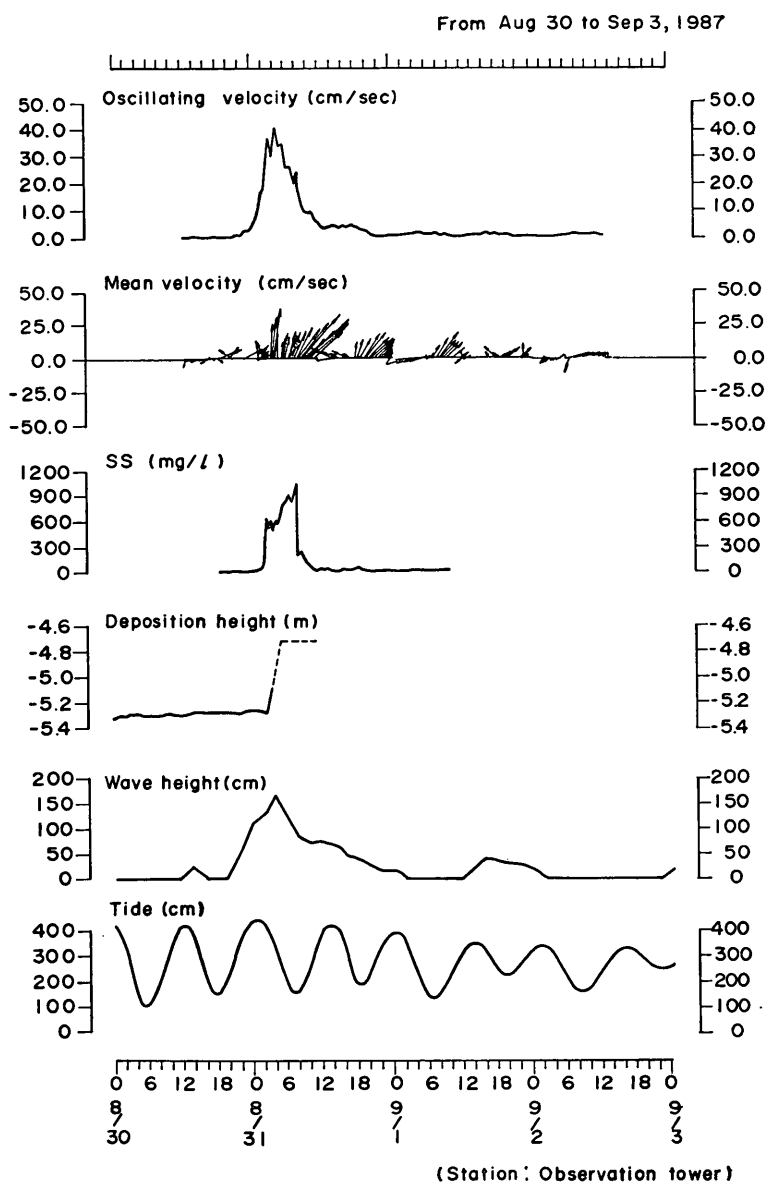
Fig. 21 Example of Measured Time Series Data from Aug. 30 to Sept. 3, 1987 at Observation Tower

December 17th, 1986 to February 19th, 1988. Trenches No. 1 and No. 2, which were not surrounded by the submerged dike, were buried up to the original level of the bottom. For trench No. 3, which is surrounded by the submerged dike, the original bottom profiele of the trench was maintained during the observation. From the figure, it is also found that the submerged dike has a considerable effect on reducing the deposition volume in trench No. 3. Around the submerged dike, no extreme erosion or deposition could be observed.

(3) External Forces and Suspended Materials

The simultaneous measurements of tides, waves, currents, turbidity, and bottom levels were carried out. Figure 21 shows the measured time series data of the oscillatory current velocity, averaged current vector, turbidity concentration, wave height, tidal level, and deposition height in trench No. 1 August 30th to September 2nd, 1987. From the figure, it is found that there is a strong correlation between the oscillatory current velocity and the turbidity concentration. Moreover, increase of the bottom level starts when wave height is large and tidal level is low. It is suspected that the bottom sediments around Kumamoto Port are eroded mainly by shear stresses caused by wind waves. Also, the bottom sediments were eroded by stormy waves when the tidal level was low.

(4) Vertical Distributions of Suspended Materials

Turbidity is measured by optical equipment. Figures 22 shows the time series of vertical distributions of turbidity measured at the observation tower. High concentration of turbidity occurred at low tide when wave height was large. Maximum concentration of turbidity was about 1,000 ppm.
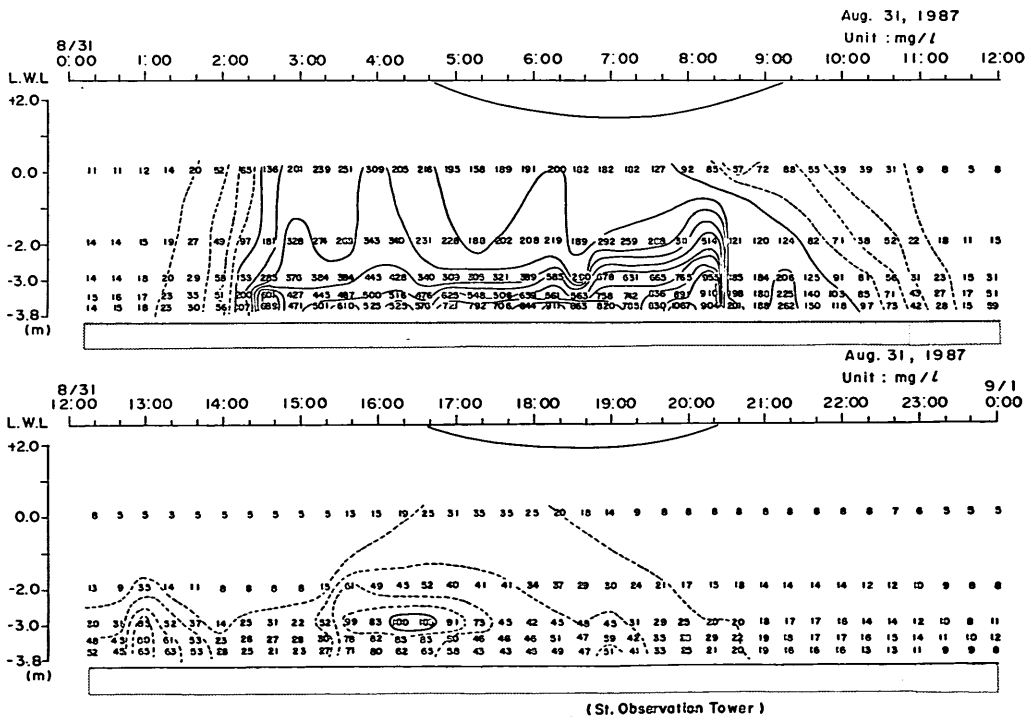


Fig. 22 Time Series of Vertical Distribution of Turbidity at Observation Tower

Hiroichi Tsuruya · Kazuo Murakami · Isao Irie

Next, the concentrations of suspended solids (SS) obtained by water sampling are described. Figures 23 shows the vertical distributions of the concentration of suspended solids at the observation tower and the pipe pile stations. A large concentration greater than 10,000 ppm was observed near the bottom. From the figure, a steep vertical gradient of SS concentration is seen.

There are discrepancies between values of turbidity and suspended solids. Turbidity is measured by optical system. On the other hand, suspended solids are measured by weighting the solid matter contained in the sampled water. Several reasons for this difference can be considered. For example, it is thought that bottom sediments were stuck to the water sampler during the survey. However, the actual reason still remains unknown.

The particle size distributions of suspended materials taken by water sampler is shown in Fig. 24. From the figure, the particle size of suspended materials at rough seas is similar to the size of bottom materials. This means that almost all bottom sediments are eroded by strong shear stresses caused by wind waves during stormy weather.

（5） Damping Factor of Waves

Waves damp during the propagation in an area of cohesive mud beds owing to the interaction between surface waves and loose mud beds. Shear stresses induced by waves are the most important factor to erode the bottom sediments in Kumamoto Port. To calculate the distribution of wave height for the whole area, it is necessary to obtain not only the data of wave transformation, but also this wave damping factor.
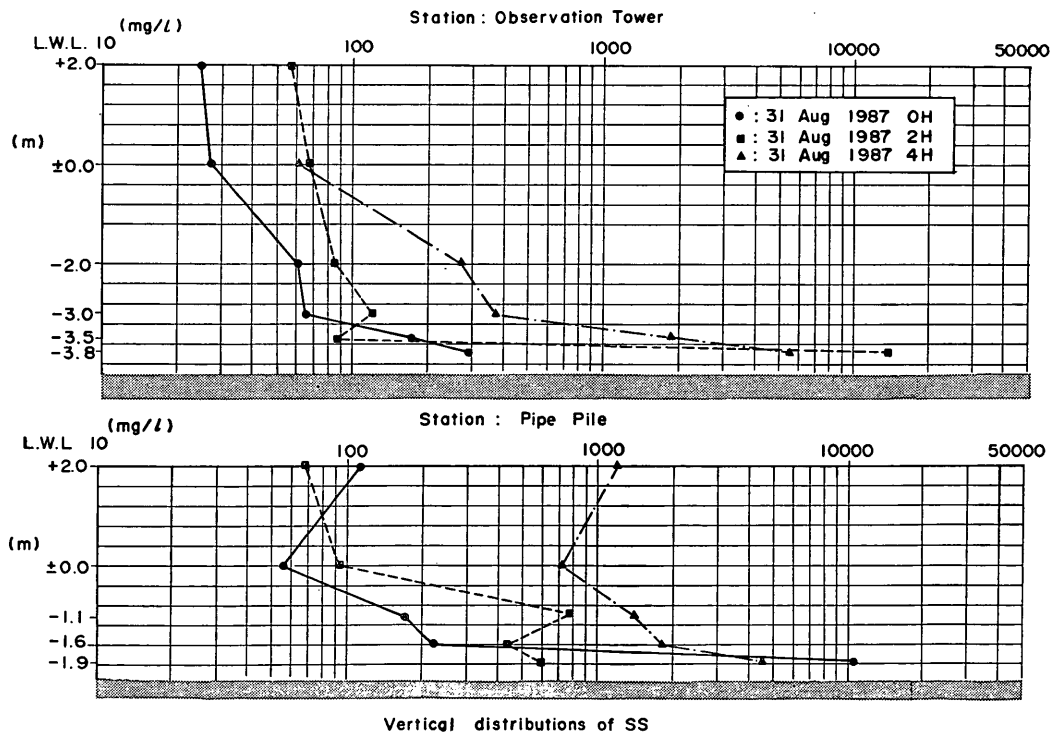


Fig. 23 Vertical Distributions of Concentration of Suspended
Solids at Observation Tower and Pipe Pile

— 30 —
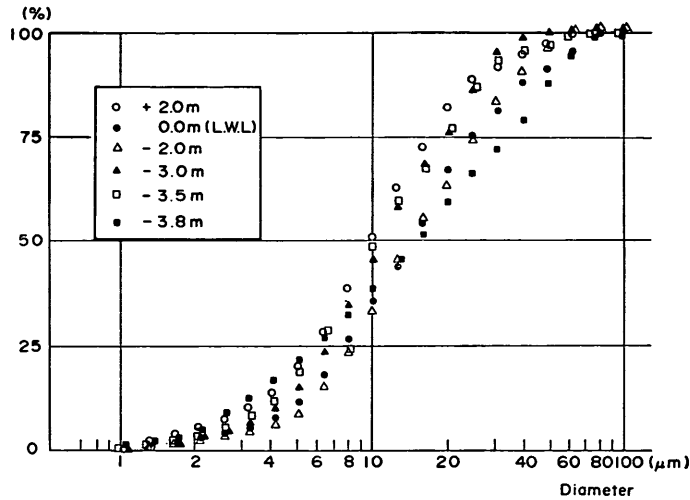
Fig. 24 Particle Size Distributions of Suspended Materials
Sampled at Various Level
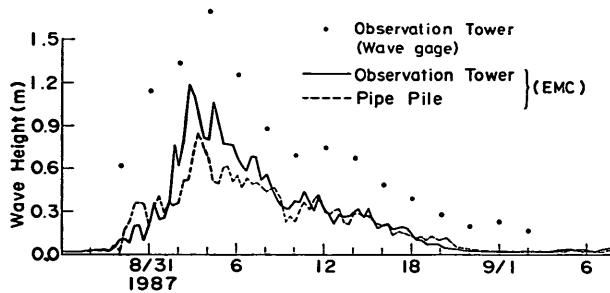
Fig. 25 Time Series of Wave Heights Measured at
Observation Tower and Pipe Pile

The damping factor was obtained from the wave heights observed at the observation tower and the pipe pile.   A wave gauge was installed on the observation tower, but not on the pipe pile.   Then wave heights are estimated by oscillatory current speed measured by the electro-magnetic current meter for both station.   Figure 25 shows the time series data of wave heights measured at the observation tower and the pipe pile.
In the figure, black dots show the wave heights measured by wave gauge at the observation tower, the solid line shows the wave heights estimated by oscillatory current at the tower, and the broken line shows the wave height at the pipe pile.   During stormy weather, wave height at the pipe pile was slightly smaller than at the observation tower. This is owing to the effect of interactions between surface water waves and the bottom mud layer.   Figure 26 shows the ratio of equivalent deep water wave height at the observation tower ($H_0$) to that of the pipe pile ($H'$).   From the results, the damping factor in Kumamoto Port is estimated to be about 0.56.
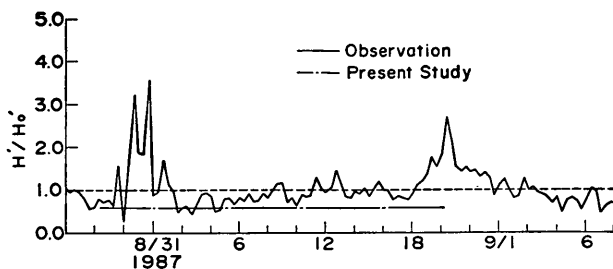
Fig. 26 Ratio of Equivalent Deepwater Wave Heights at
Observation Station to That of Pipe Pile

# 4. Calibration

## 4.1 General Description

Figure 19 shows the abrupt depositions occurred on February 6th and September 1st. We adopt the deposition on September 1st as the representative case for the calibration. Part of port facilities had been constructed at that time. The "Kumamoto Port Ohashi" bridge with a length of 872 m, connecting the offshore port and the city, a wharf with a length of 300 m, and part of the revetment for a reclaimed were completed.

The area for calculation is divided into five areas from the first to the fifth. Mesh sizes are 300 m, 100m, and 100/3 m for each area from the first to the third respectively. For the fourth and the fifth area, the mesh size is 100/9 m. Arrangement of the mesh for the first area is presented in Fig. 27. Magnifield meshes for the second area are
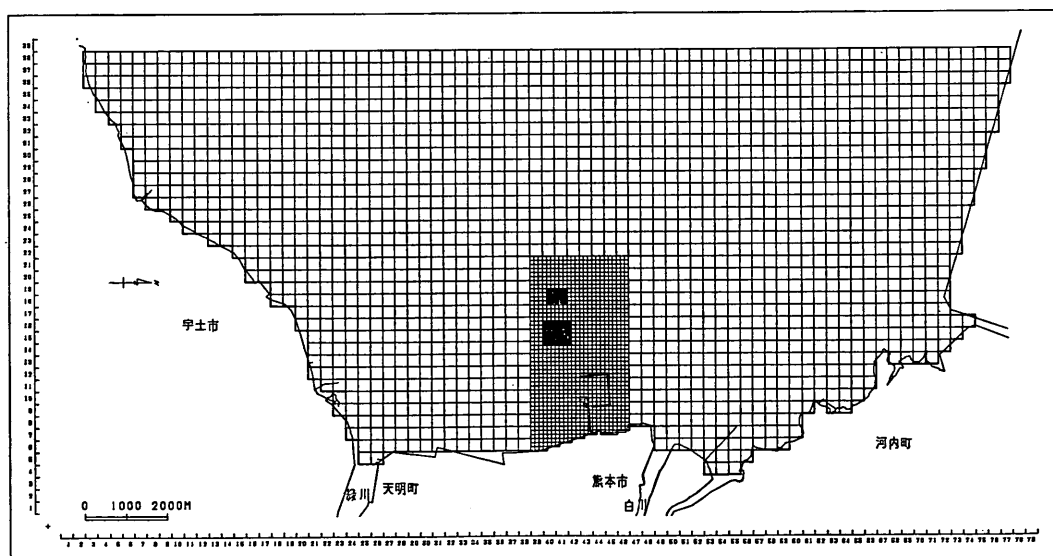


Fig. 27 Mesh Map for the First Area
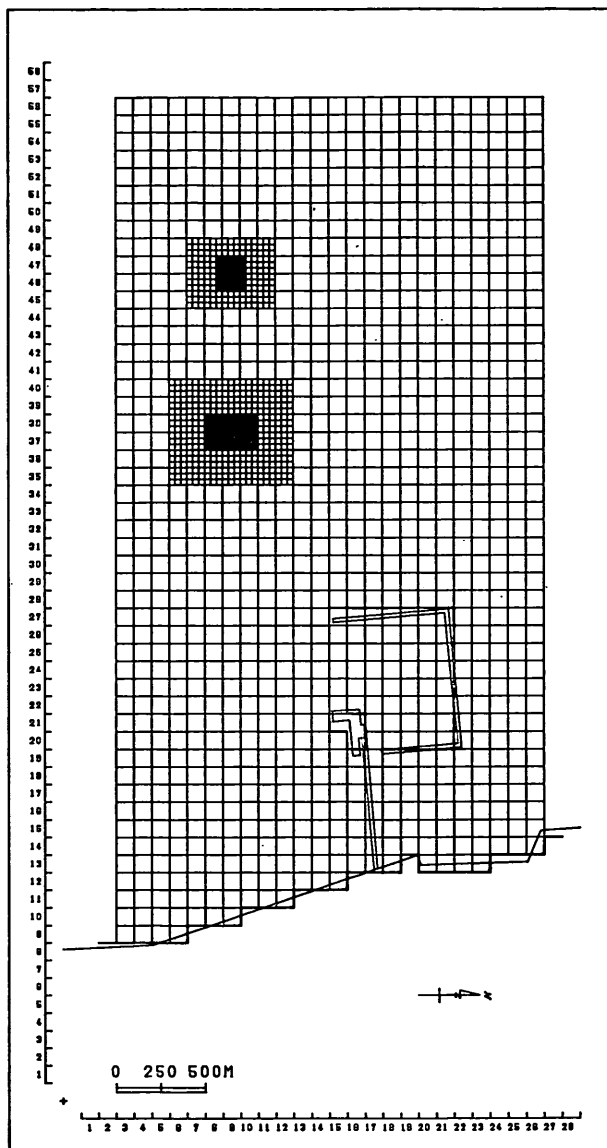
格子図（第2領域）
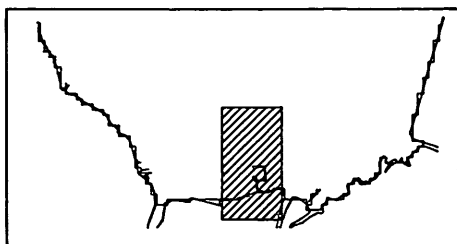
Fig. 28  Mesh Map for the Second Area

shown in Fig. 28. The third area is separated into two parts. Within them, there exist the fourth and the fifth area. Figure 29 shows the fourth area that includes No. 2 and 3 trenches. The trench on the left side is surrounded by a submerged dike. The fifth area shown in Fig. 30 includes trench No. 1. Numbers in the figures mean the water depths from the mean water level (MWL) in decimeter units. The mean water level is 2.45 m above the datum level (DL) as explained in Fig. 9. The smallest mesh size is 11.1 m. The present nested grid model can treat the composite mesh arrangement of rough and fine meshes. Therefore, calculation, which includes the small area with special interest, can be efficiently conducted.

The number of layers is seven as already shown in Fig. 2. The thickness of the first layer is 3 m. The tidal range is included within the first layer so that the shore-line moves within this layer according to the tidal level. The thickness of the layer is set at 0.5 m for layers 2, 3, 4, and 5 because the submerged dikes in the future plan will be set between these layers. The number of layers in the first area are shown in Fig. 31. Near the coast, there is a shallow area which consists of only one layer. At the deeper site, on the other hand, the number of layers is seven. From the bottom sampling data, constituent rate of mud and sandy mud is decided as shown in Table 4. The boundary between mud and sandy mud beds is shown in Fig. 32. Onshore sides from the boundaries are the sandy mud areas.
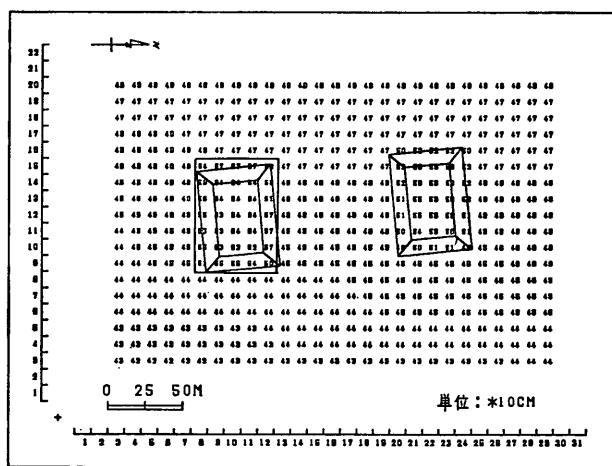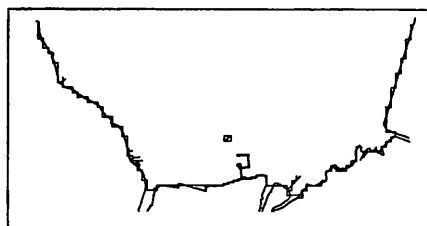


Fig. 29 Water Depths within the Fourth Area
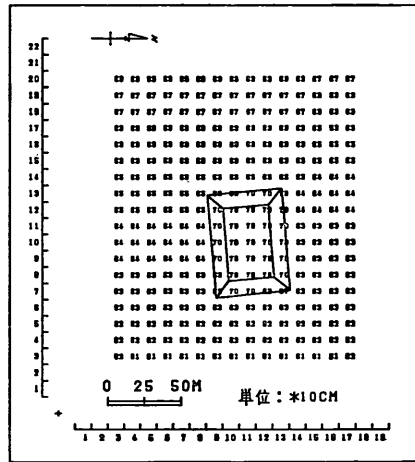
水深（第5領域）
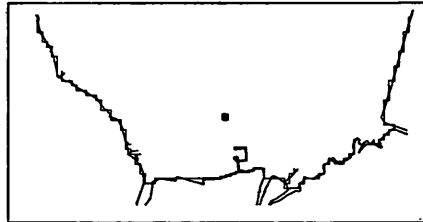
Fig. 30  Water Depths within the Fifth Area
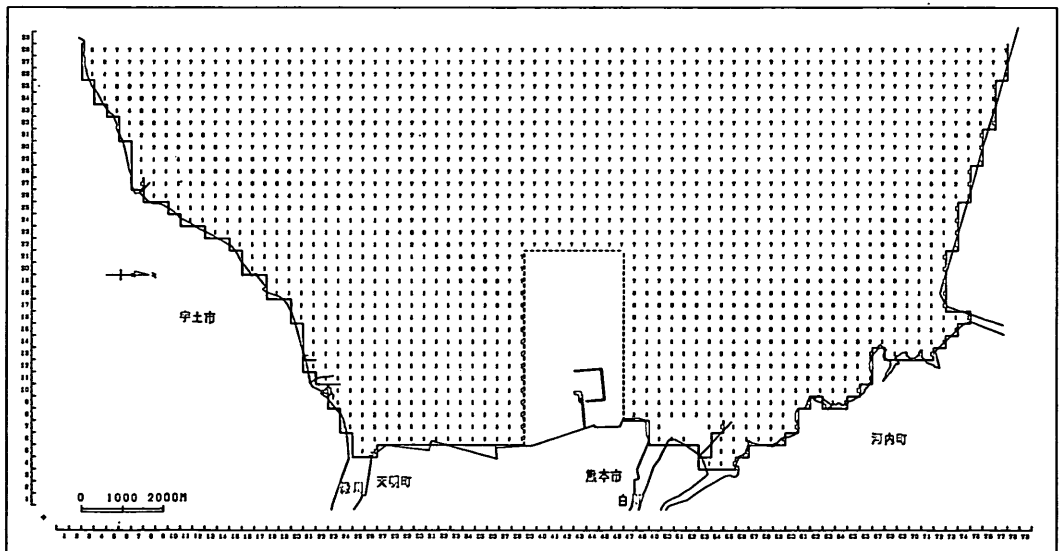


Fig. 31  Numbers of Layer for the First Area
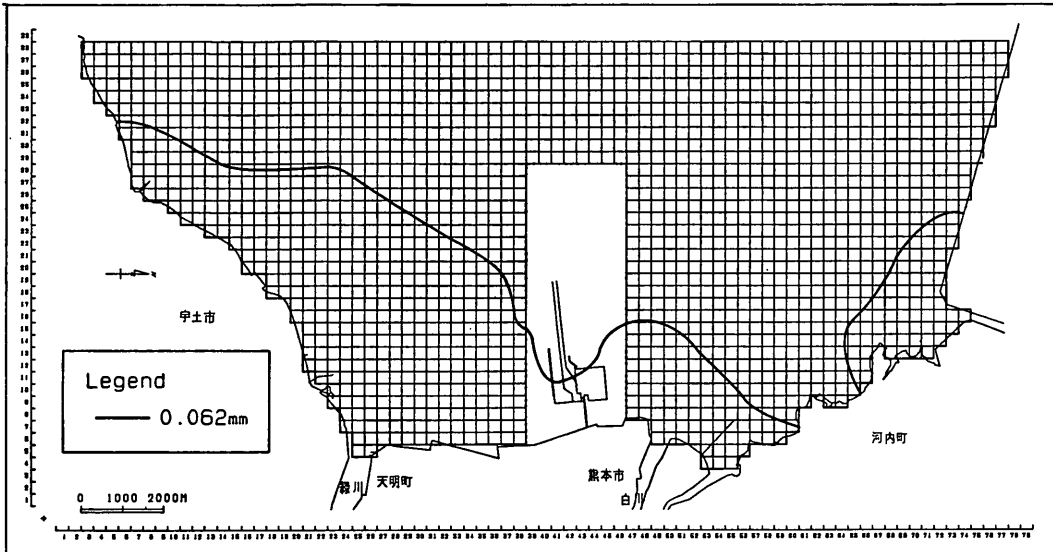
**Fig. 32** Boundary between Mud and Sandy Mud

**Table 4** Constituent Rate of Mud and Sandy Mud

|  | Mud ($D_{50} < 0.062$mm) | Sandy mud ($D_{50} > 0.062$mm) | |
|---|---|---|---|
| Grain size | 0.020mm | 0.020mm | 0.24mm |
| Percentage | 100% | 20% | 80% |

## 4.2 Damping of Surface Waves

The observed wave heights at the observation tower and the pipe pile were previously shown in Chapter 3.

The ratio of the equivalent wave height at the pipe pile to that at the observation tower is shown in Fig. 26.

The predicted value by the multi-layered viscous fluid model (*Tsuruya et al.*, 1987) is shown as a dash-dot line in Fig. 26. When wave heights are large, i. e., from 2:00 to 6:00 a. m., August 31st (see Fig. 25), the theoretical value agrees dosely with the observation. In the calculation, the depth of the mud layer and water content are set to at 10cm and 200%, respectively.

Calculated rate of mass transport is shown in Figs. 33, 34, and 35 as a unit of cm³/s/cm.
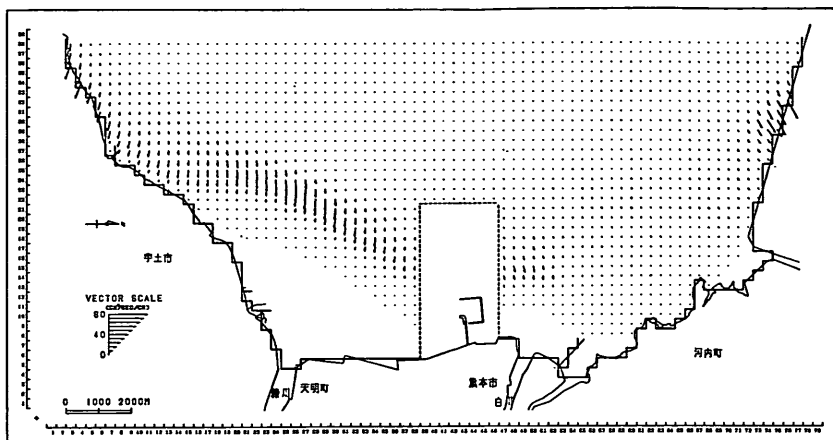
Fig 33  Calculated Mass Transport Volume (First Area)
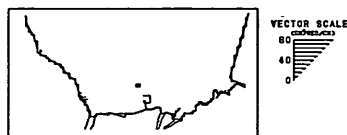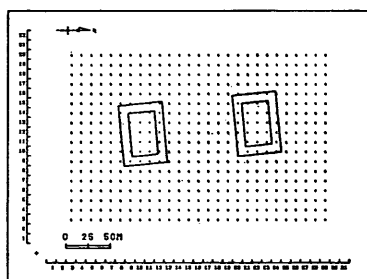


Fig. 34  Calculated Mass Transport Volume
(Fourth Area)
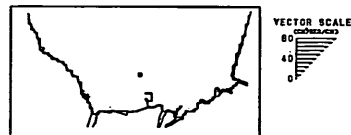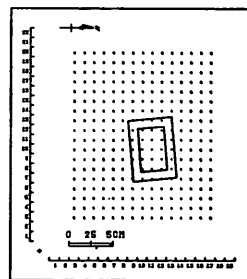
Fig. 35  Calculated Mass Transport Volume
(Fifth Area)

## 4.3  Tidal Currents

In the calculation of tidal currents, measured velocities at the open boundary are given as the boundary conditions (*Katoh et al.*, 1979).

We can recognize from Table 3 that the maximum significant wave height is 1.69 m at 4:00 a.m., August 31st.  At 2:00 a.m. when the value of $SS$ starts to increase (see Figs. 21 and 22), the significant wave height and period are 1.33 m and 4.2 s, respectively.  Relating these items to the deposition, wave conditions are decided to be as follows: $H_{1/3}=1.25$ m, $T_{1/3}=4$ s, direction of the wave is WSW, and their duration is 6 hours.  It can be said from Fig. 21 that when waves are large, the tidal level is low.  Therefore, waves are operated from 15:00 to 21:00 in the calculation as shown in Fig. 36  Only tidal current is calculated from 0:00 to 15:00.  Calculations of erosion, diffusion, and settlement is conducted from 15:00 to 27:00.  All the calculations are finished at time 27:00.
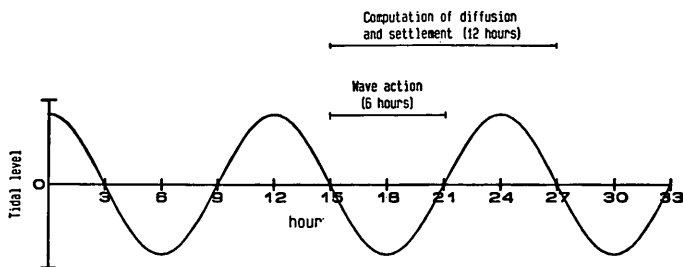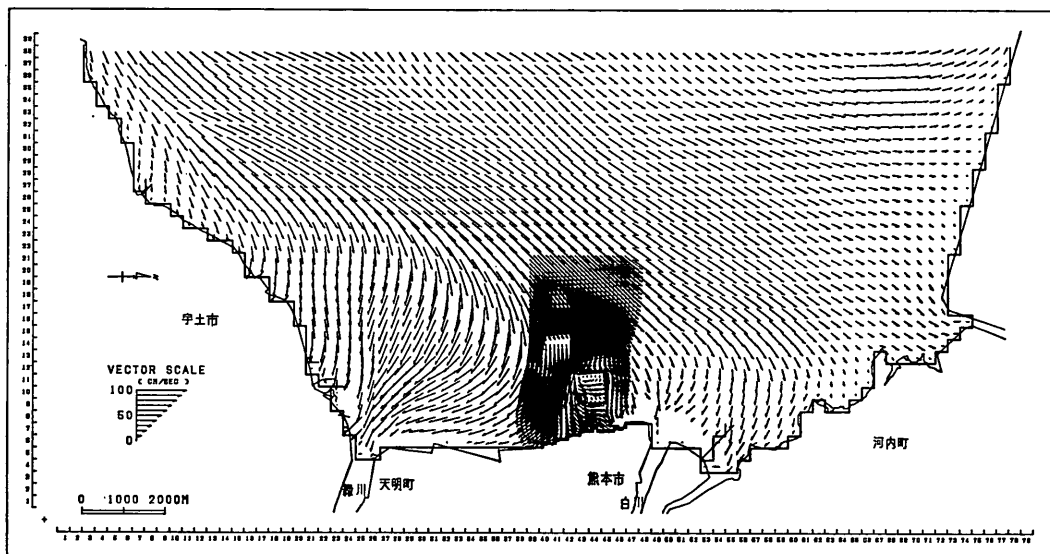
Fig. 36 Time Table of Calculation



Fig. 37 Calculated Velocity Distribution for the First Layer
at the Maximum Flood Tide

An example of the calculated tidal current distribution is shown in Fig. 37. Velocities in the second area where the mesh is three times smaller than that of the first area are expressed together with the velocities for the first area.

## 4.4 Vertical Distribution of Suspended Solids

The calculated vertical distributions of suspended solids (SS) are shown in Figs. 38 and 39 along the center lines of trenches No. 2 and No. 3, respectively The time is 21:00 and the current direction is from offshore to onshore. Figure 38 (without submerged dike) for trench No. 2 shows the vertical distributions of SS similar to that in Fig. 23. In Fig. 39, which is for trench No. 3, vertical distributions of SS are almost uniform because of the existence of the submerged dike and the concentration at the bottom layer is smaller than that of the previous case.
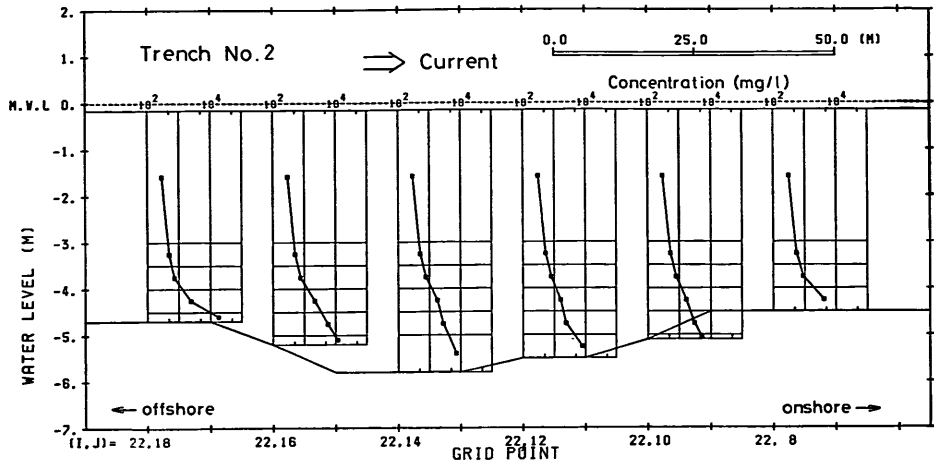
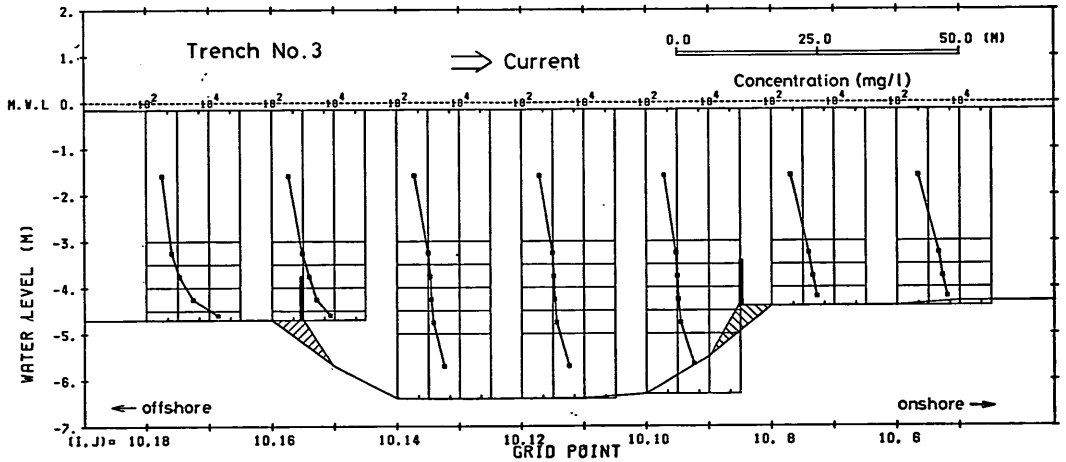Fig. 38 Calculated Vertical Distributions of SS (Trench No. 2)



Fig. 39 Calculated Vertical Distributions of SS (Trench No. 3)

## 4.5 Deposition Rates

Measureed deposition heights during rough seas from August 31st to September 1st within three trenches are listed in Table 5 together with the water content.

In the calculation of erosion, the critical shear stress $\tau_e$ was set at 0.1 (Pa) after *Murakami et al.,* (1989) and the constant $M$ was varied until the reasonable deposition heights are obtained. The calculated deposition heights are listed in Table 6. The upper row shows the contribution from deposition only and the lower one shows the total amount by both deposition and mass transport owing to wave action. Comparing with Table 5, the calculated total deposition heights agree with the measured one. The

Table 5   Deposition Heights and Water Contents
within Three Trenches
(Aug. 29–Sept. 2, 1987)

|  | Trench No. 1 | Trench No. 2 | Trench No. 3 |
|---|---|---|---|
| Deposition Height (cm) | 63 | 60 | −2 |
| Water Content (%) | 231 | 189 | 192 |

Table 6   Calculated Result of Deposition Heights

|  | Trench No. 1 | Trench No. 2 | Trench No. 3 |
|---|---|---|---|
| Deposition (cm) | 63. 4 | 39. 8 | 4. 0 |
| Deposition + Mass Transport (cm) | 74. 6 | 53. 4 | 4. 0 |

value of $M$ thus estimated is 1. 2kg/m²/min.   According to *van Leussen and Dronkers* (1988), the range of $M$ is 0. 006~0. 24 kg/m²/min.   We have a larger value of $M$ for the present model than usual.   However, as the model dose not include every process in the field, we must finally calibrate the calculated value by the field data.   Therefore, we concluded that the present model could reproduce the deposition heights in the field.

## 5.   Application to Future Plans of Kumamoto Port

### 5.1   Tidal Currents
   We have two cases for the future plans as shown in Figs. 40 and 41.   Figure 40 corresponds to the tentative plan that will be completed by the end of March 1990. This is named as future plan 1.   The final plan is shown in Fig. 41 and is named as future plan 2.   The mesh arrangement is the same for both figures.   The smallest mesh size is 100/3 m (=33.3 m), and the region with this mesh is named the third area. The mesh size of the coarser area is 100 m.   This area is named the second area.   The coarsest mesh size as shown in Fig. 27 is 300 m and the area is called the first area.   In
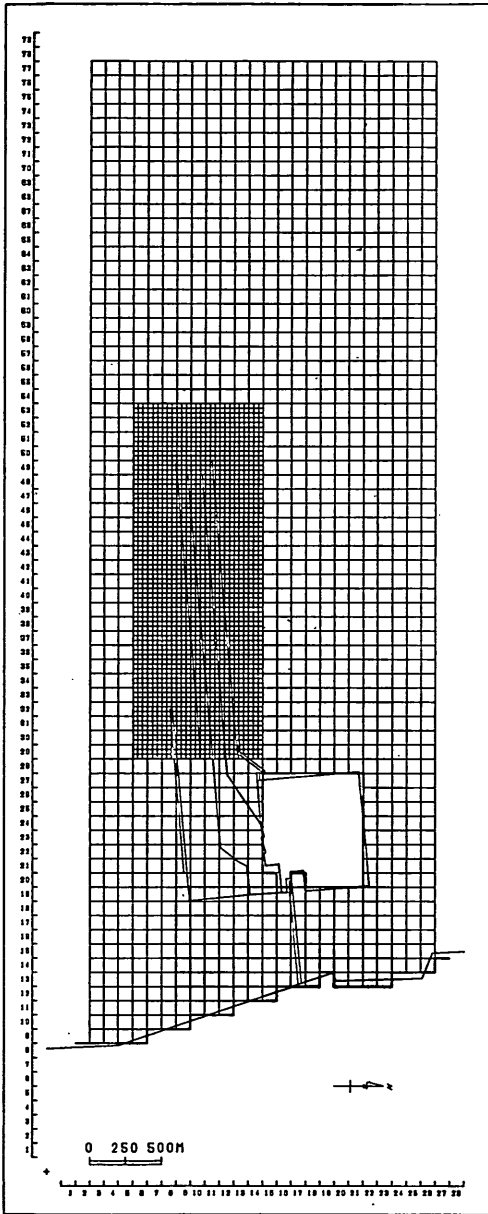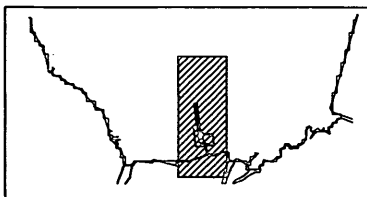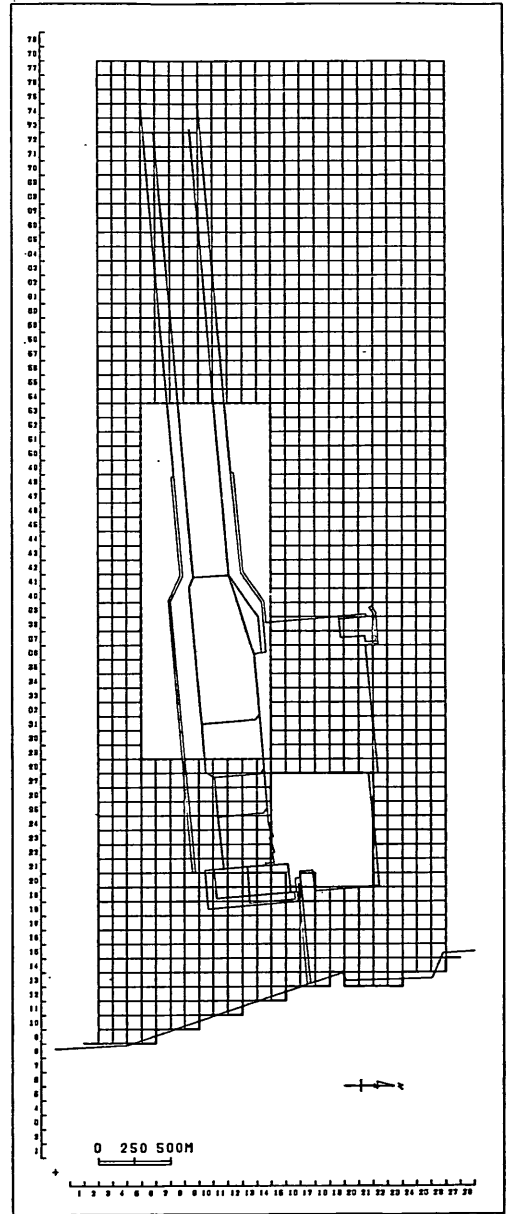
格子図 (第2領域)

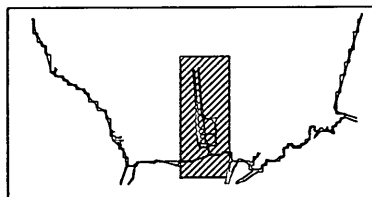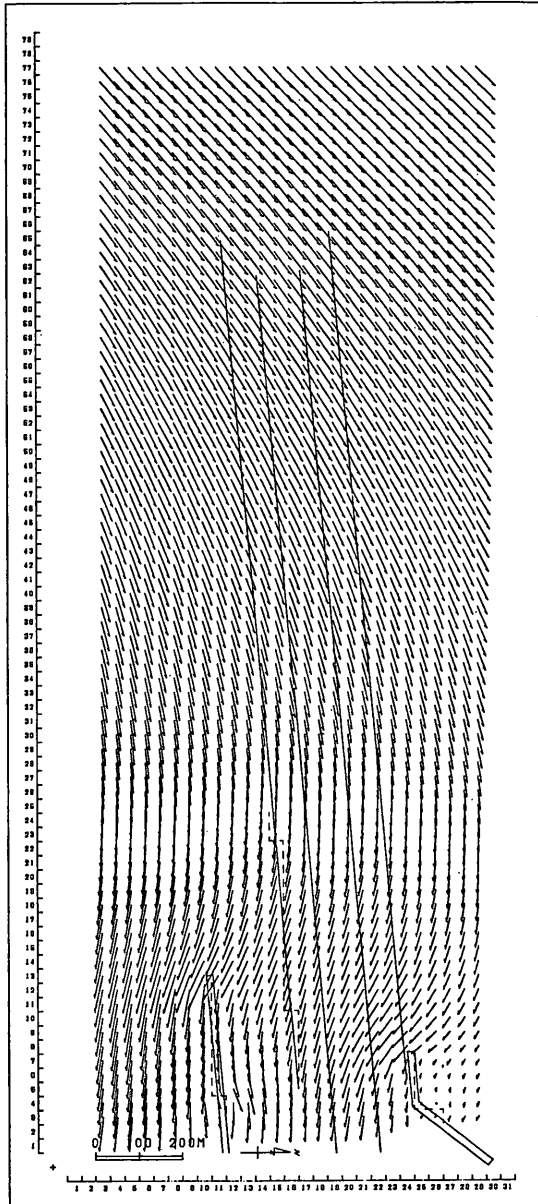Fig. 40 Mesh Map for Future Plan 1

格子図 (第2領域)

Fig. 41 Mesh Map for Future Plan 2

ベクトル図（第3領域・第1層・21．00HOUR）

ベクトル図（第3領域・第3層・21．00HOUR）

**Fig. 42** Calculated Velocity Distribution for the First Layer (With Submerged Dikes)
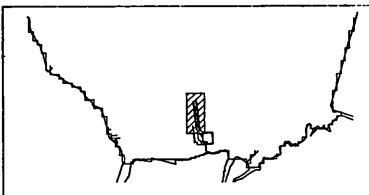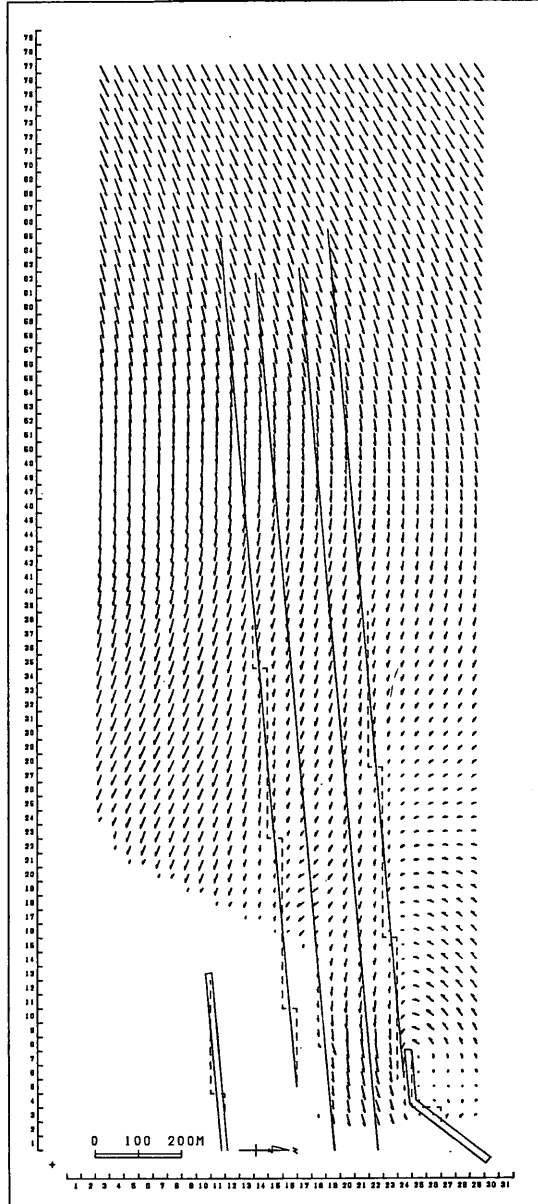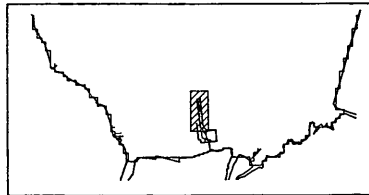
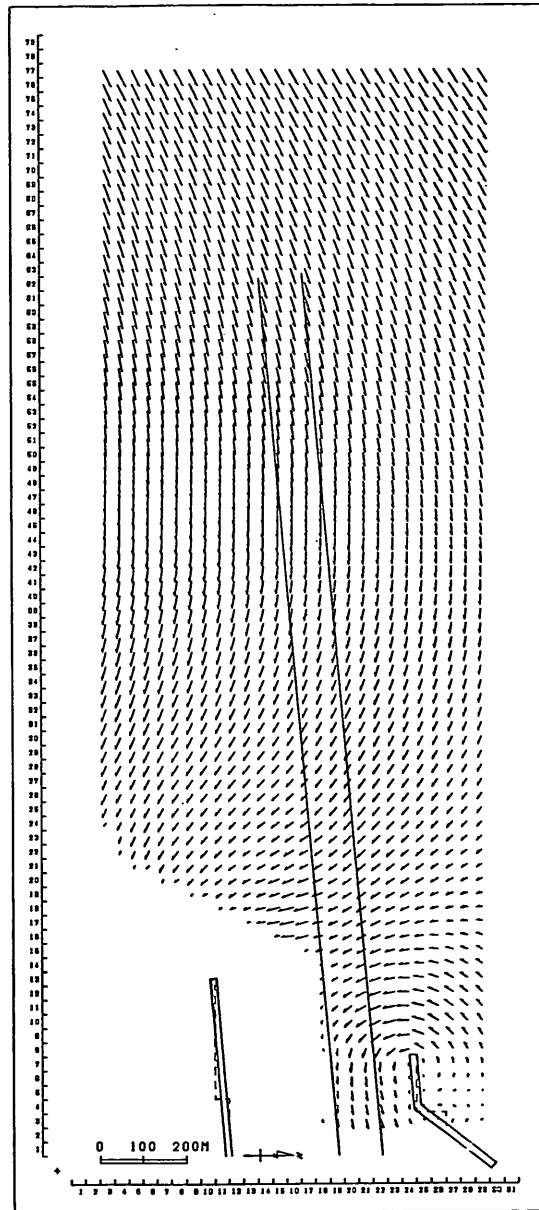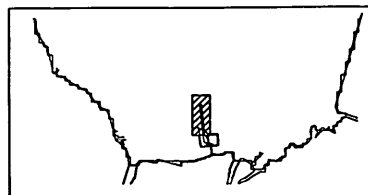**Fig. 43** Calculated Velocity Distribution for the Third Layer (With Submerged Dikes)

ベクトル図（第3領域・第3層・21.00HOUR）

Fig. 44  Calculated Velocity Distribution for the
         Third Layer (Without Submerged Dikes)

the third area of Fig. 40, the access channel is 100 m wide and is shown as the inner parallel lines. The depth of the access channel is 4.5 m. The outer lines parallel to the access channel are submerged dikes which are 2,000 m in length. The width of the access channel for future plan 2 (Fig. 41) is 250 m and the depth is 10 m. Submerged dikes are also shown as the parallel lines outside the access channel. In both cases, the height of the submerged dikes is 1 m. Conditions of the calculation are exactly the same as the calibration case.

Figure 42 shows the calculated tidal current distribution at 21 hours for the first layer of the third area in future plan 1. Figure 43 shows the tidal current distribution at the same time but for th third layer. The submerged dikes are shown as the broken lines. Velocities of the first layer are faster than that of the third layer and the directions of the currents are different. As the height of the submerged dikes is set at 1 m from the bottom, elevation of the submerged dikes in offshore site is deeper than in onshore site. In Fig. 43, we can recognize that because of the existence of the submerged dikes in the third layer, velocities near them become small. Figure 44 shows the velocity distribution for the third area in the case without submerged dikes. Comparing with Fig. 43, we can notice that velocities near the breakwaters and along the access channel increase if we don't place submerged dikes.

## 5.2 Amount of Deposition

The calculated deposition heights inside the access channel are added together to get the volume of deposition for each area as shown in Figs. 45 and 46. It is assumed that the water content of the deposited mud is 200%. The amount of deposition in each area is shown in Fig. 47. The maximum deposition occurs at area E. The reducing effect of deposition by submerged dikes is about 23% for area E and 47% for area G. The calculated volume includes mass transport by waves. In the calculation, there is no limitation for erosion. Although bottom change for each mesh is not shown, erosion is large between the submerged dikes. In the field, the bottom material in the deeper position will be harder than that of the bottom surface. The solid triangles in Fig. 47 show the case in which the critical shear stress of the bed material for erosion between the submerged dikes is a function of the depth from the bed surface. The critical shear stress for erosion from the bed surface to a depth of 5 cm is set at 0.1 Pa and 0.3 Pa for mud deeper than 5 cm. The average depth of deposition and the volume of deposition are listed in Table 7. The amount of decrease in the volume of deposition owing to the submerged dikes is about 30%.

The calculated vertical distributions of suspended sediment concentration along the line I-I' in Fig. 46 is shown in Fig. 48. This case is without submerged dikes. Outside the access channel, the concentration at the bottom layer is two orders of magnitude greater than that at the surface layer. Within the access channel, however, the difference of the concentration is smaller than that outside the access channel.

Figures 49 and 50 show the partition of the access channels and anchorages of future plan 2. The calculated amount of depositions within the access channel are added together like future plan 1. The calculated result of the volume of deposition is shown in Fig 51. It can be concluded that the total deposition will decrease about 23% if 1 m height submerged dikes will settle along the access channel.
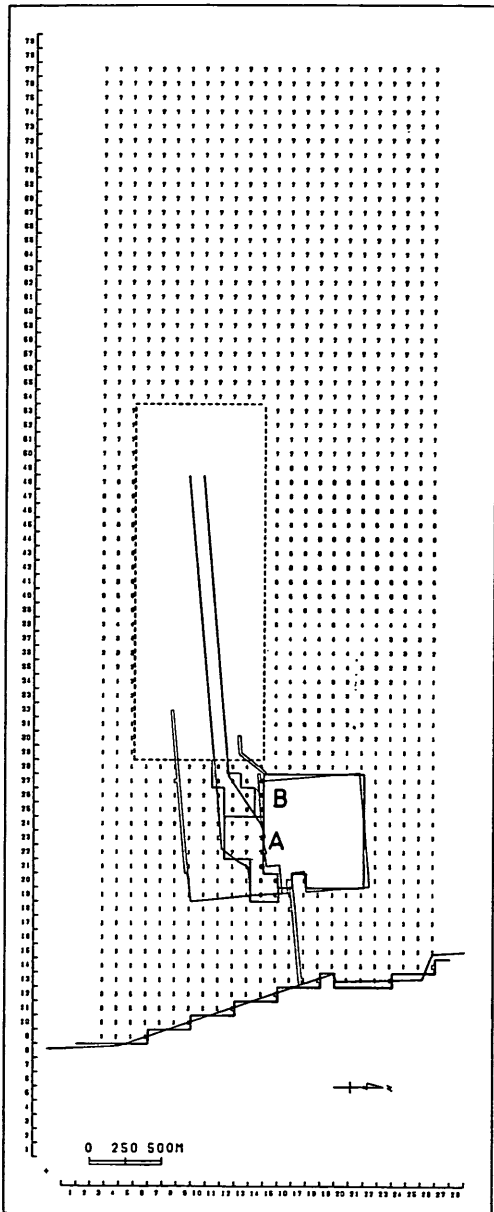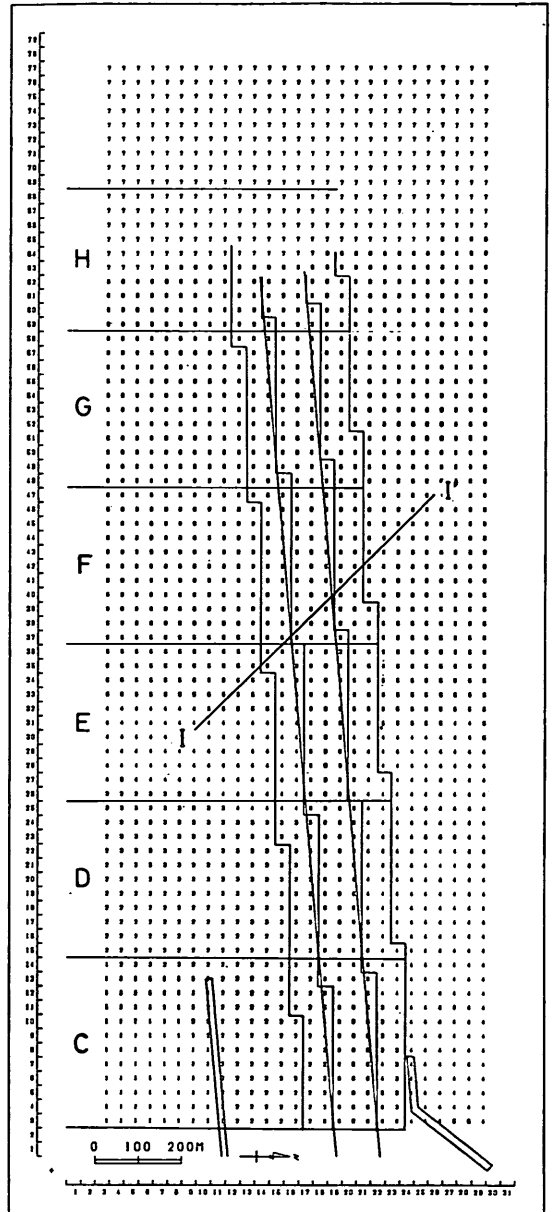
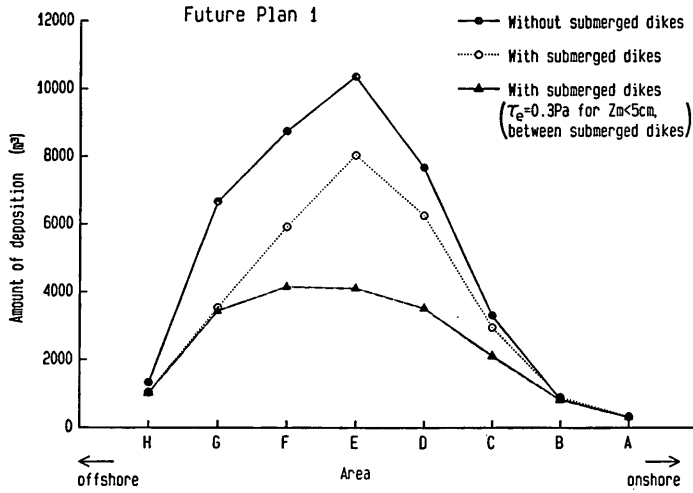Fig. 45  Division of Anchorage

Fig. 46  Division of Access Channel

Fig. 47   Amount of Deposition in Each Area
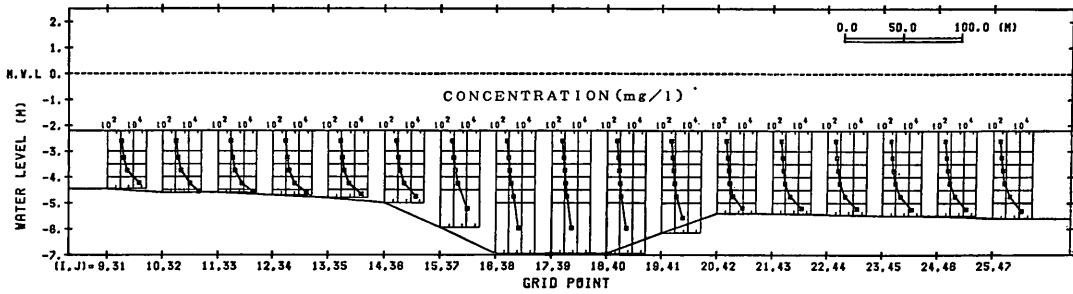


Fig. 48   Vertical Distribution of Suspended Solids (I-I′ Line)

Table 7  Volume of Deposits in Future Plan 1 (in Access Channel)

| Area (Numbers of Mesh) | (without submerged dike) | | (with submerged dike) | |
|---|---|---|---|---|
| | Average depth of deposition (cm) | Volume of deposition (m³) | Average depth of deposition (cm) | Volume of deposition (m³) |
| H | 2.98 | 1,205 | 3.03 | 1,042 |
| (31) | 3.99 | 1,330 | 3.03 | 1,042 |
| G | 13.85 | 5,233 | 8.93 | 3,374 |
| (34) | 17.66 | 6,672 | 9.38 | 3,544 |
| F | 19.90 | 7,517 | 15.17 | 5,731 |
| (34) | 23.15 | 8,745 | 15.69 | 5,927 |
| E | 26.02 | 9,539 | 21.51 | 7,887 |
| (33) | 28.25 | 10,357 | 21.90 | 8,030 |
| D | 19.74 | 7,456 | 16.31 | 6,162 |
| (34) | 20.31 | 7,671 | 16.55 | 6,253 |
| C | 7.83 | 3,221 | 7.09 | 2,915 |
| (37) | 8.05 | 3,311 | 7.19 | 2,956 |
| B | 1.19 | 834 | 1.28 | 895 |
| (7) | 1.19 | 834 | 1.28 | 895 |
| A | 0.22 | 308 | 0.23 | 325 |
| (14) | 0.22 | 308 | 0.23 | 325 |
| Total | 35,313 | | 28,331 | |
| | 39,228 | | 28,972 | |

Upper: Deposition only.
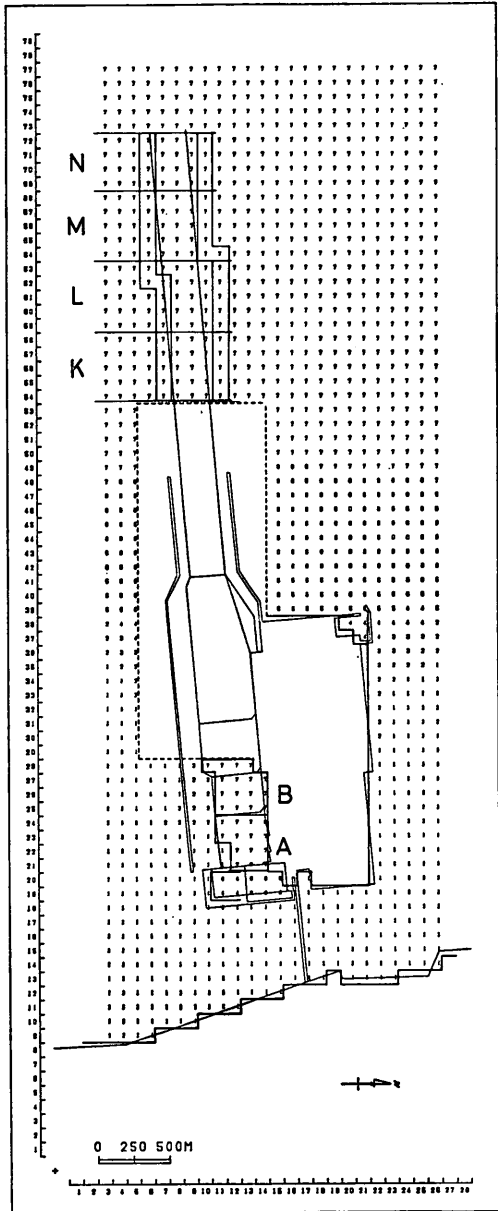Lower: Deposition and mass transport.

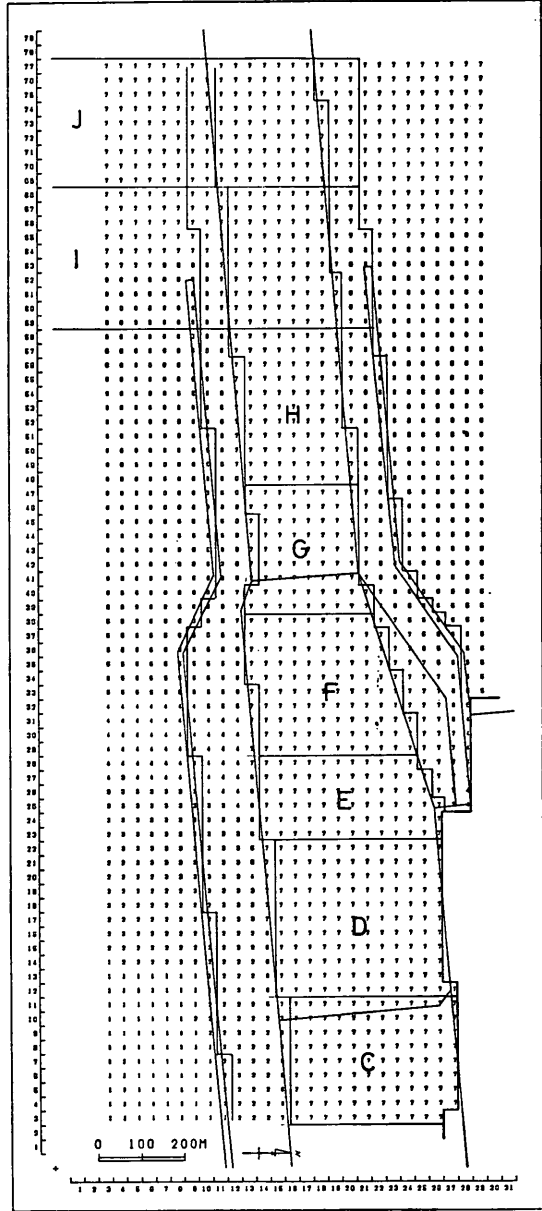Fig. 49 Division of Anchorage and Access Channel



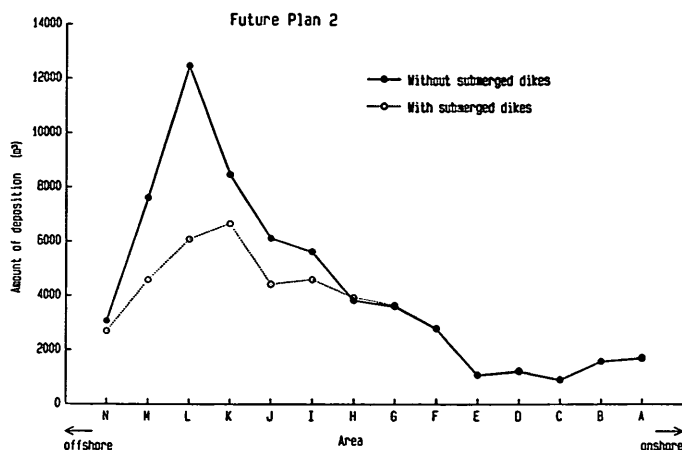Fig. 50 Division of Anchorage and Access Channel

Fig. 51　Amount of Deposition in Each Area

## 6.　Discussion

The present model is a diffusion model.　The validity of the model is examined by comparing the deposition height within three trenches.　The calibrated parameter is only one, namely, the constant of erosion $M$. Siltation mechanism is so complicated that every process cannot be included in the model, and the accumulation of parameters from the laboratories and another tests would result in serious mistakes.　The present model, in this sense, needs the actual deposition data in the field.　This is more or less common to every model.　The present model does not take fluid mud into account.
As fluid mud is so dense and easy to move, access channels in a coast area will suffer the inflow of it provided the fluid mud is formed sufficiently.　The formation of the fluid mud is important but it is difficult to confirm its existence and the detailed characteristics are not yet well explained.　Also, investigations about the flowing behavior of fluid mud around the strudture should be done for the fluid mud model.

## 7.　Conclusious

Three-dimensional multi-layered level model with nested grid is developed for the calculation of siltation.　To investigate the effect of submerged dikes on the siltation, the water depth is divided into seven horizontal layers.　Vertical distridutions of mud concentration are also reproduced in the model.　A supercomputer is used for the complicated and large scale calculations.
After the calibration of deposition heights within three trenches, calculations for the future plans of Kumamoto Port are conducted.　The amount of decrease in the volume of deposition owing to submerged dikes was 30% for future plan 1 and 23% for future plan 2.　　　　　　　　　　　　　　　　*(Received on November 30, 1989)*

## References

1) Bijker, E. W. (1980) : Sedimentation in channels and trenches, *Proc. 17th Conf. Coastal Engineering,* pp. 1708-1718.
2) Bijker, E. W. (1982) : Physical models for coastal morphology and harbour problems, *Hydraul. model marit. Eng.,* pp. 87-94.
3) Dyer, K. R. (1986) : Coastal and estuarine sediment dynamics, John Wiley & Sons, 342p.
4) Goda, Y. (1985) : Random seas and design of maritime structure, University of Tokyo Press, 323p.
5) Irie, I and Y. Kuriyama (1988) : Reproduction of sedimentation in harbours by combined physical / mathematical modeling, *Proc. IAHR Symp. Math. Modeling Sediment Transp. Coast. Zone, IAHR,* pp. 79-88.
6) Jonsson, I. G. (1966) : Wave boundary layers and friction factors, *Proc. 10th Coastal Engg. Conf.,* Tokyo Vol. 1, CH. 10.
7) Katoh, K., N. Tanaka and K. Nadaoka (1979) : Tidal simulation on tidal marsh and numerical forecasting of is topographic deformation, *Report of the Port and Harbour Research Institute.* pp. 3-76. *(in Japanese)*
8) Mehta, A. J. (1986) : Characterization of cohesive sediment properties and transport processes in estuaries, in Mehta A. J. (Ed), Estuarine Cohesive Dynamics, Lec. Notes Coastal Estuarine Stud. 14, pp. 290-325.
9) Murakami, K., F, Suganuma and H. Sasaki (1989) : Experimental investigation on erosion and deposition of fine cohesive sediments in an annular rotation channel, *Report of the Port and Harbour Research Institute,* Vol. 28, No. 1, pp. 43-76 *(in Japanese).*
10) Partheniades, E. (1965) : Erosion and deposition of cohesive soils. *Journal of Hydraulics Res.,* ASCE, Vol. 91, No. 1, pp. 105-139.
11) Rubey, W. W. (1933) : Settling velocities of gravel, sand and silt particles, *Amer. Jour. Sci.,* Vol. 25, pp 325-338.
12) Sheng, Y. P. and W. Lick (1979) : The transport and resuspension of sediments in a shallow lake, *J. Geopys. Res.,* Vol. 84, pp. 1809-1826.
13) Takayama, T. (1981) : Wave diffraction and wave height distribution inside a harbour, *Tech. Note of PHRI,* No. 369, 140p. *(in Japanese).*
14) Tanaka, H. and N. Shuto (1981) : Friction coefficient for a wave-current coexistent system, *Coastal Engineering in Japan,* Vol. 24, pp. 105-128.

15) Thorn, M. F. C. (1981) : Physical processes of siltation in tidal channels, *Proc. Hrdraulic Modelling Applied to Maritime Engineering Problems*. ICE, London, pp. 47 -55.

16) Tsuruya, H., S. Nakano and J. Takahama (1987) : Interactions between surface waves and a multi-layered mud bed, *Report of the Post and Harbour Research Institute*, Vol. 26, No. 5, pp. 137-173.

17) Van Leussen, W. and J. Dronkers (1988) : Physical Process in Esturies : An Introduction, in Dronkers, J. and W. van Leussen (ed), Physical processes in estuaries, Springer-Verlag, 560p.

18) Yatsushiro Port Construction Office (1988) : Report of investigation on countermeasure against siltation in Kumamoto Port, Fourth District Port Construction Bureau, Ministry of Transport, 128p. *(in Japanese)*.